

ON SCHRÖDINGERIZATION BASED QUANTUM ALGORITHMS FOR LINEAR DYNAMICAL SYSTEMS WITH INHOMOGENEOUS TERMS

SHI JIN ^{*}, NANA LIU [†], AND CHUWEN MA [‡]

Abstract. We analyze the Schrödingerization method for quantum simulation of a general class of non-unitary dynamics with inhomogeneous source terms. The Schrödingerization technique, introduced in [S. Jin, N. Liu and Y. Yu, Phys. Rev. Lett., 133 (2024), 230602], transforms any linear ordinary and partial differential equations with non-unitary dynamics into a system under unitary dynamics via a warped phase transition that maps the equations into a higher dimension, making them suitable for quantum simulation. This technique can also be applied to these equations with inhomogeneous terms modeling source or forcing terms, or boundary and interface conditions, and discrete dynamical systems such as iterative methods in numerical linear algebra, through extra equations in the system. Difficulty arises with the presence of inhomogeneous terms since they can change the stability of the original system.

In this paper, we systematically study—both theoretically and numerically—the important issue of recovering the original variables from the Schrödingerized equations, even when the evolution operator contains unstable modes. We show that, even with unstable modes, one can still construct a stable scheme; however, to recover the original variable, one needs to use suitable data in the extended space. We analyze and compare both the discrete and continuous Fourier transforms used in the extended dimension and derive corresponding error estimates, which allow one to use the more appropriate transform for specific equations. We also provide a smoother initialization for the Schrödingerized system to gain higher-order accuracy in the extended space. We homogenize the inhomogeneous terms with a stretch transformation, making it easier to recover the original variable. Our recovery technique also provides a simple and generic framework to solve general ill-posed problems in a computationally stable way.

Key words. quantum algorithms, Schrödingerization, non-unitary dynamics, differential equations with inhomogeneous terms.

MSC codes. 65M70, 65M30, 65M15, 81-08

1. Introduction. Quantum computing is considered a promising candidate to overcome many limitations of classical computing [17, 38, 39], one of which is the curse of dimensionality. It has been shown that quantum computers could potentially outperform the most powerful classical computers, with polynomial or even exponential speed-up, for certain types of problems [18, 34].

In this paper, we focus on the general linear dynamical system as stated below

$$(1.1) \quad \frac{d}{dt}\mathbf{u} = A(t)\mathbf{u}(t) + \mathbf{b}(t), \quad \mathbf{u}(0) = \mathbf{u}_0,$$

where $\mathbf{u}, \mathbf{b} \in \mathbb{C}^n$, $A \in \mathbb{C}^{n \times n}$ is a time-dependent matrix. This system includes ordinary differential equations (ODEs) and partial differential equations (PDEs). In the continuous representation, $A(t)$ is the differential operator; in the spatially discrete version, a PDE becomes a system of ODEs. Classical algorithms become inefficient or even prohibitively expensive due to large dimension n whereas quantum methods can

^{*} School of Mathematical Sciences, Shanghai Jiao Tong University, Institute of Natural Sciences, Shanghai Jiao Tong University, Ministry of Education, Key Laboratory in Scientific and Engineering Computing, Shanghai Jiao Tong University, Shanghai 200240, China. (shijin-m@sjtu.edu.cn)

[†] Institute of Natural Sciences, Shanghai Jiao Tong University, Ministry of Education, Key Laboratory in Scientific and Engineering Computing, Shanghai Jiao Tong University, University of Michigan-Shanghai Jiao Tong University Joint Institute, Shanghai 200240, China. (nanaliu@sjtu.edu.cn)

[‡] School of Mathematical Sciences, Shanghai Jiao Tong University, Institute of Natural Sciences, Shanghai Jiao Tong University, Shanghai 200240, China. (chuwenii@lsec.cc.ac.cn)

possibly significantly speed up the computation. Therefore, the design for quantum simulation algorithms for solving general dynamical systems – including both ODEs and PDEs – is important for a wide range of applications, for example, molecular dynamics simulations, and high dimensional and multiscale PDEs.

The development of quantum algorithms with up to exponential advantage excel in unitary dynamics, in which $A(t) = iH(t)$ with $H = H^\dagger$ (where \dagger represents complex conjugate) and $\mathbf{b} = \mathbf{0}$ in (1.1), which is also known as the Hamiltonian simulation. Many efficient quantum algorithms for Hamiltonian simulation have been developed in the literature (e.g., [2, 3, 5, 6, 7, 8, 9, 10, 11, 14, 16, 33, 36, 43]). However, most dynamical systems in applications involve non-unitary dynamics, making them unsuitable for quantum simulation. A very recent proposal for such problems is based on Schrödingerization, which converts non-unitary dynamics to Schrödinger-type equations with unitary dynamics. This is achieved by a warped phase transformation that maps the system to one higher dimension. The original variable \mathbf{u} can then be recovered via integration or pointwise evaluation in the extra-dimensional space. This technique can be applied in both qubit-based [29, 30, 31] and continuous-variable frameworks [24], with the latter being suitable for analog quantum computing. The method can also be extended to solve open quantum systems in a bounded domain with artificial boundary conditions [26], physical and interface conditions [23], and even discrete dynamical systems such as iterative methods in numerical linear algebra [25].

For non-Hermitian $H(t)$, the Schrödingerization first decomposes it into the Hermitian and anti-Hermitian parts:

$$(1.2) \quad A = H_1 + iH_2, \quad H_1 = (A + A^\dagger)/2, \quad H_2 = (A - A^\dagger)/(2i),$$

where $H_1 = H_1^\dagger, H_2 = H_2^\dagger$, followed by the warped phase transformation for the H_1 part. A basic assumption for the application of the Schrödingerization technique is that the eigenvalues of H_1 need to be negative [30, 31]. This corresponds to the stability of solution to the original system (1.1). When there is an inhomogeneous term $\mathbf{b}(t)$, one needs to enlarge the system so as to deal with just a homogeneous system. However, the new H_1 corresponding to the enlarged system will have positive eigenvalues—which will be proved in this paper—violating the basic assumption of the Schrödingerization method. We address this important issue in this paper.

We show that even if some of the eigenvalues of H_1 are positive, the Schrödingerization method can still be applied. However, in this case one needs to be more careful when recovering the original variable \mathbf{u} . Specifically, one can still obtain \mathbf{u} by using an appropriate domain in the new extended space, which is not ‘distorted’ by spurious right-moving waves generated by the positive eigenvalues of H_1 .

We will also analyze both discrete and continuous Fourier transformations used in the extended dimension. The corresponding error estimates for the discretization will be established. A smoothed initialization is also introduced to provide a higher order accuracy in approximations in the extended dimension (see Remark 4.5). Furthermore, a stretching transformation is used to lower the impact of positive eigenvalues of H_1 , which makes it easier to recover the original variables. We also show that the stretch coefficient does not affect the error of the Schrödingerization discretization.

The rest of the paper is organized as follows. In section 2, we give a brief review of the Schrödingerization approach for general homogeneous linear ODEs and two different Fourier discretizations in the extended space for this problem. In section 3, we show the conditions for correct recovery from the warped transformation, even when

there exist positive eigenvalues of H_1 , which triggers potential instability for the extended dynamical system. We also show the implementation protocol on quantum devices. The error estimates and complexity analysis are established in section 4. In section 5, we consider the inhomogeneous problems and show that the enlarged homogeneous system will contain unstable modes corresponding to positive eigenvalues of H_1 . The recovering technique introduced in section 3 can be used to deal with this system. Finally, we show the numerical tests in section 6.

Throughout the paper, we restrict the simulation to a finite time interval $t \in [0, T]$. The notation $f \lesssim g$ stands for $f \leq Cg$ where C is a positive constant independent of the numerical mesh size and time step. Moreover, we use a 0-based indexing, i.e. $j = \{0, 1, \dots, N-1\}$, or $j \in [N]$. Additionally, we utilize the notation $|j\rangle \in \mathbb{C}^N$ to represent a vector where the j -th component being 1 and all other components are 0. We denote the identity matrix and null matrix by I and O , respectively. The dimensions of these matrices should be clear from the context; otherwise, I_N refers to the N -dimensional identity matrix. Without specific statements, $\|\mathbf{b}\|$ denotes the Euclidean norm defined by $\|\mathbf{b}\| = (\sum_i |b_i|^2)^{1/2}$ and $\|A\|$ denotes matrix 2-norms defined by $\|A\| = \sup_{\|\mathbf{x}\|=1} \|A\mathbf{x}\|$. The vector-valued quantities are denoted by boldface symbols, such as $\mathbf{L}^2(\Omega) = (L^2(\Omega))^n$.

2. A review of Schrödingerization for general linear dynamical systems.

In this section, we briefly review the Schrödingerization approach for general linear dynamical systems. Defining an auxiliary vector function $\mathbf{r}(t) \equiv \sum_i |i\rangle \in \mathbb{R}^n$ that remains constant in time, system (1.1) can be rewritten as a homogeneous system

$$(2.1) \quad \frac{d}{dt} \begin{bmatrix} \mathbf{u} \\ \mathbf{r} \end{bmatrix} = \begin{bmatrix} A & B \\ O & O \end{bmatrix} \begin{bmatrix} \mathbf{u} \\ \mathbf{r} \end{bmatrix}, \quad \begin{bmatrix} \mathbf{u}(0) \\ \mathbf{r}(0) \end{bmatrix} = \begin{bmatrix} \mathbf{u}_0 \\ \mathbf{r}_0 \end{bmatrix},$$

where $B = \text{diag}\{b_1, b_2, \dots, b_n\}$ and $\mathbf{r}_0 = \sum_i |i\rangle \in \mathbb{R}^n$. Therefore, without loss of generality, we assume $\mathbf{b} = \mathbf{0}$ in (1.1). Since any matrix can be decomposed into a Hermitian term and an anti-Hermitian one as in (1.2), Equation (1.1) can be expressed as

$$(2.2) \quad \frac{d}{dt} \mathbf{u} = H_1 \mathbf{u} + iH_2 \mathbf{u}, \quad \mathbf{u}(0) = \mathbf{u}_0.$$

The Schrödingerization method introduced in [29, 31] assumes that *all eigenvalues of H_1 are negative*. This corresponds to assuming that the original dynamical system (1.1) is *stable*. Using the warped phase transformation $\mathbf{w}(t, p) = e^{-p} \mathbf{u}$ for $p > 0$ and symmetrically extending the initial data to $p < 0$, Equation (2.2) is converted to a system of linear convection equations:

$$(2.3) \quad \frac{d}{dt} \mathbf{w} = -H_1 \partial_p \mathbf{w} + iH_2 \mathbf{w}, \quad \mathbf{w}(0) = e^{-|p|} \mathbf{u}_0.$$

When the eigenvalues of H_1 are all negative, the convection term of (2.3) corresponds to a wave moving from the right to the left, thus one does not need to impose a boundary condition for \mathbf{w} at $p = 0$. One does, however, need a boundary condition on the right hand side. Since \mathbf{w} decays exponentially in p , one just needs to select $p = p^*$ large enough, so \mathbf{w} at this point is essentially zero and a zero incoming boundary condition can be used at $p = p^*$. Then \mathbf{u} can be recovered via

$$(2.4) \quad \mathbf{u}(t) = \int_0^{p^*} \mathbf{w}(t, p) dp \quad \text{or} \quad \mathbf{u}(t) = e^p \mathbf{w}(t, p) \quad \text{for any} \quad 0 < p < p^*.$$

2.1. The discrete Fourier transform for Schrödingerization. We denote $\sigma(H_1)$ the set of eigenvalues of H_1 . To discretize the p domain, we choose a large enough domain $p \in \Omega_p = (-\pi L, \pi L)$, $L > 0$, such that

$$(2.5) \quad e^{-\pi L + 2\lambda_{\max}^+(H_1)T + R} \leq \epsilon, \quad e^{-\pi L + \lambda_{\max}^-(H_1)T + \lambda_{\max}^+(H_1)T + R} \leq \epsilon,$$

where ϵ is the desired accuracy, $R \geq 1$ is the length of the recovery region with $e^R = \mathcal{O}(1)$, and

$$\begin{aligned} \lambda_{\max}^+(H_1) &= \max \left\{ \sup_{0 < t < T} \{|\lambda| : \lambda \in \sigma(H_1(t)), \lambda > 0\}, 0 \right\}, \\ \lambda_{\max}^-(H_1) &= \max \left\{ \sup_{0 < t < T} \{|\lambda| : \lambda \in \sigma(H_1(t)), \lambda < 0\}, 0 \right\}. \end{aligned}$$

We note that (2.5) is intended for numerical analysis and is quite mild for numerical tests. Specifically, it implies that $e^{-\pi L + \lambda_{\max}^+(H_1)T} \lesssim \epsilon$ and $e^{-\pi L + \lambda_{\max}^-(H_1)T} \lesssim \epsilon$. Furthermore, as implied by (2.4), the discretization error may grow exponentially with p . To mitigate this instability, we impose the condition $e^R = \mathcal{O}(1)$ on the recovery interval. Then, we set the uniform mesh size $\Delta p = 2\pi L/N_p$ where N_p is a positive even integer and the grid points are denoted by $-\pi L = p_0 < \dots < p_{N_p} = \pi L$. Define the vector \mathbf{w}_h the collection of the function \mathbf{w} at these grid points by

$$\mathbf{w}_h = \sum_{k \in [N_p]} \sum_{j \in [n]} w_{kj} |k\rangle |j\rangle.$$

where w_{kj} is denotes the approximation to $w_j(t, p_k)$. The 1-D basis functions for the Fourier spectral method are usually chosen as

$$(2.6) \quad \phi_l(p) = e^{i\mu_l(p + \pi L)}, \quad \mu_l = (l - N_p/2)/L, \quad l \in [N_p].$$

Using (2.6), we define

$$(2.7) \quad \Phi = (\phi_{jl})_{N_p \times N_p} = (\phi_l(p_j))_{N_p \times N_p}, \quad D_p = \text{diag}\{\mu_0, \dots, \mu_{N_p-1}\}.$$

Considering the Fourier spectral discretisation on p , one easily gets

$$(2.8) \quad \frac{d}{dt} \mathbf{w}_h = -i(P \otimes H_1) \mathbf{w}_h + i(I_{N_p} \otimes H_2) \mathbf{w}_h.$$

Here P is the matrix representation of the momentum operator $-i\partial_p$ and defined by $P = \Phi D_p \Phi^{-1}$. Through a change of variables $\tilde{\mathbf{w}}_h = [\Phi^{-1} \otimes I_n] \mathbf{w}_h$, one gets

$$(2.9) \quad \begin{cases} \frac{d}{dt} \tilde{\mathbf{w}}_h = -i(D_p \otimes H_1 - I_{N_p} \otimes H_2) \tilde{\mathbf{w}}_h = -iH^d \tilde{\mathbf{w}}_h, \\ \tilde{\mathbf{w}}_h(0) = (\Phi^{-1} \otimes I_n) \mathbf{w}_h(0). \end{cases}$$

At this point, a quantum algorithm for Hamiltonian simulation can be constructed for the above linear system (2.9). If H_1 and H_2 are usually sparse, then the Hamiltonian $H = D_p \otimes H_1 - I_{N_p} \otimes H_2$ inherits the sparsity.

2.2. The continuous Fourier transform for Schrödingerization. In the previous section, $\partial_p \mathbf{w}(t, p)$ is first discretized in p by the discrete Fourier transform.

Here, we consider the continuous Fourier transform of $\mathbf{w}(p)$ and its inverse transformation defined by

$$\hat{\mathbf{w}} := \mathcal{F}(\mathbf{w})(\xi) = \frac{1}{2\pi} \int_{\mathbb{R}} e^{i\xi p} \mathbf{w}(p) dp, \quad \mathbf{w} := \mathcal{F}^{-1}(\hat{\mathbf{w}})(p) = \int_{\mathbb{R}} e^{-i\xi p} \hat{\mathbf{w}}(\xi) d\xi.$$

The continuous Fourier transform in p for (2.3) gives

$$(2.10) \quad \begin{aligned} \frac{d}{dt} \hat{\mathbf{w}} &= i\xi H_1 \hat{\mathbf{w}} + iH_2 \hat{\mathbf{w}} = i(\xi H_1 + H_2) \hat{\mathbf{w}}, \\ \hat{\mathbf{w}}(0) &= \frac{1}{\pi(1 + \xi^2)} \mathbf{u}_0. \end{aligned}$$

We can first consider the truncation of the ξ -domain to a finite interval $[-X, X]$ with

$$(2.11) \quad X^{-1} = \mathcal{O}(\epsilon),$$

where ϵ is the desired accuracy. Then canonical Hamiltonian simulation methods can be applied to the following unitary dynamics

$$(2.12) \quad \begin{cases} \frac{d}{dt} \check{\mathbf{w}}_h = i(D_\xi \otimes H_1 + I_{N+1} \otimes H_2) \check{\mathbf{w}}_h = iH^c \check{\mathbf{w}}_h, \\ \check{\mathbf{w}}_h(0) = \boldsymbol{\xi}_h \otimes \mathbf{u}_0, \end{cases}$$

where $D_\xi = \text{diag}\{\xi_0, \xi_1, \dots, \xi_N\}$ and $\boldsymbol{\xi}_h = \sum_{j=0}^N \frac{|j\rangle}{\pi(1 + \xi_j^2)}$.

It is also possible to consider the continuous Fourier transform without truncation in the ξ domain. This is possible when considering implementation on analog quantum devices [24]. In this case, instead of finite-dimensional matrices or states we define infinite dimensional vectors $|w(t)\rangle \equiv \int \mathbf{w}(t, p) |p\rangle dp$, which are acted on by infinite dimensional operators \hat{p} and $\hat{\xi}$, where $[\hat{p}, \hat{\xi}] = iI$. These infinite dimensional states and operators have natural meaning in the context of analog quantum computation, where they can represent for example quantum states of light or superconducting modes. If we let $|p\rangle$ and $|\xi\rangle$ denote the eigenvectors of \hat{p} and $\hat{\xi}$ respectively, then $\langle p|\xi\rangle = \exp(ip\xi)/\sqrt{2\pi}$. Let \mathcal{F} denote the continuous Fourier transform acting on these infinite dimensional states with respect to the auxiliary variable p , then $\mathcal{F}|p\rangle = |\xi\rangle$. Note that this \mathcal{F} operation also has a natural interpretation in quantum systems and can be implemented in its continuous form. These $\{|p\rangle\}_{p \in \mathbb{R}}$ and $|\xi\rangle_{\xi \in \mathbb{R}}$ eigenstates each form a complete eigenbasis so $\int dp |p\rangle \langle p| = I = \int d\xi |\xi\rangle \langle \xi|$. Here the quantised momentum operator $\hat{\xi}$ is also associated with the derivative $\hat{\xi} \leftrightarrow -i\partial/\partial p$ and it is straightforward to show $i\hat{\xi}|w(t)\rangle = |\partial w/\partial p\rangle$.

In this case, Eq. (2.10) does not transform into Eq. (2.12), but rather to

$$(2.13) \quad \begin{aligned} \frac{d|w(t)\rangle}{dt} &= i(\hat{\xi} \otimes H_1 + I \otimes H_2)|w(t)\rangle, \\ |w(0)\rangle &= \int \frac{1}{\pi(1 + \xi^2)} |\xi\rangle d\xi \mathbf{u}_0. \end{aligned}$$

3. Recovery of the original variables and implementations on quantum devices . The purpose of this section is to show the rigorous conditions of the recovery \mathbf{u} from \mathbf{w} and the implementation on a quantum device. We consider the more general case, namely here we will *allow the eigenvalues of H_1 to be non-negative*, which is the case for many applications and extensions of the Schrödingerization method, for example systems with inhomogeneous terms [29, 31], boundary value and interface problems [26, 23], and iterative methods in numerical linear algebra [25].

3.1. Recovery of the original variable. Since H_1 is Hermitian, assume it has n real eigenvalues, ordered as

$$(3.1) \quad \lambda_1(H_1) \leq \lambda_2(H_1) \leq \cdots \leq \lambda_n(H_1), \quad \text{for all } t \in [0, T].$$

Next we define the solution to the time-dependent Hamiltonian system (2.10) as

$$\hat{\mathbf{w}}(t) = \mathcal{U}_{t,0}(\xi) \hat{\mathbf{w}}(0),$$

where the unitary operator $\mathcal{U}_{t,s}$ is defined by the time-ordering exponential, $\mathcal{T}e$, via Dyson's series [32],

$$(3.2) \quad \mathcal{U}_{t,s} = \mathcal{T}e^{i \int_s^t H(y) dy} = I + \sum_{n=1}^{\infty} \frac{i^n}{n!} \int_s^t dt_1 \cdots \int_s^t dt_n \mathcal{T}[H(t_1)H(t_2) \cdots H(t_n)],$$

where $\mathcal{T}[H(t_1)H(t_2) \cdots H(t_n)] = H(t_{i_1})H(t_{i_2}) \cdots H(t_{i_n})$ with $t_{i_1} > t_{i_2} \geq \cdots \geq t_{i_n}$, and $\mathcal{U}_{t,s}$ satisfies

$$\frac{d}{dt} \mathcal{U}_{t,s} = iH(t)\mathcal{U}_{t,s}, \quad \mathcal{U}_{t,s} = \mathcal{U}_{t,s'}\mathcal{U}_{s',s}, \quad \mathcal{U}_{t,s}^\dagger = \mathcal{U}_{s,t}.$$

THEOREM 3.1. *Assume the eigenvalues of H_1 satisfy (3.1), the solution of (1.1) can be recovered by*

$$(3.3) \quad \mathbf{u} = e^p \mathbf{w}(t, p), \quad \text{for any } p \geq p^\diamond,$$

where $p^\diamond \geq \lambda_{\max}^+(H_1)T$, or recovered by using the integration,

$$(3.4) \quad \mathbf{u} = e^p \int_p^\infty \mathbf{w}(q) dq, \quad \text{for any } p \geq p^\diamond.$$

Proof. Following the proof in [19, Theorem 5, section 7.3], we conclude that the solution of (2.3) is unique and given by

$$(3.5) \quad \mathbf{w}(t, p) = \int_{\mathbb{R}} \hat{\mathbf{w}}(t, \xi) e^{-i\xi p} d\xi = \int_{\mathbb{R}} \frac{\mathcal{U}_{t,0}(\xi) \mathbf{u}_0}{\pi(1 + \xi^2)} e^{-i\xi p} d\xi.$$

It is sufficient to prove that for any $p > p^\diamond$, $\mathbf{w}(t, p)$ satisfies

$$\frac{d}{dt} \mathbf{w}(t, p) = A(t) \mathbf{w}(t, p), \quad \mathbf{w}(0, p) = e^{-p} \mathbf{u}_0.$$

It is obvious that the initial condition holds by letting $t = 0$ in (3.5). Since $p > \lambda_{\max}^+(H_1)T$, for any $t \in [\delta, T]$, where $\delta > 0$, one has $\lambda(H_1) - p/t \leq 0$. According to [4, Lemma 5], there holds

$$(3.6) \quad \mathcal{P} \int_{\mathbb{R}} \frac{\mathcal{U}_{t,0}(\xi) e^{-i\xi p}}{1 - i\xi} d\xi = \mathcal{P} \int_{\mathbb{R}} \frac{1}{1 - i\xi} \mathcal{T}e^{i \int_0^t (\xi(H_1(s) - p/t) + H_2(s)) ds} d\xi = 0,$$

where \mathcal{P} stands for the Cauchy principal value of the integral. Differentiating $\mathbf{w}(t)$ with respect to t gives

$$(3.7) \quad \begin{aligned} \frac{d}{dt} \mathbf{w}(t, p) &= \mathcal{P} \int_{\mathbb{R}} \frac{i(\xi H_1(t) + H_2(t)) \mathcal{U}_{t,0}(\xi)}{\pi(1 + \xi^2)} \mathbf{u}_0 e^{-i\xi p} d\xi \\ &= -\mathcal{P} \int_{\mathbb{R}} \frac{H_1(t) \mathcal{U}_{t,0}(\xi) e^{-i\xi p}}{\pi(1 - i\xi)} \mathbf{u}_0 d\xi + \mathcal{P} \int_{\mathbb{R}} \frac{A(t) \mathcal{U}_{t,0}(\xi) \mathbf{u}_0}{\pi(1 + \xi^2)} e^{-i\xi p} d\xi \\ &= A(t) \mathbf{w}(t, p). \end{aligned}$$

Considering δ can be small enough, (3.7) holds for any $t \in (0, T]$. The proof is finished by the fact that $\mathbf{w}(t, p) = e^{-p}\mathbf{u}(t)$ for $p \geq p^\diamond$. \square

Remark 3.2. When $\lambda(H_1) \leq 0$, we recover \mathbf{u} through (3.5) by choosing $p = 0$, and obtain

$$(3.8) \quad \mathbf{u} = \int_{\mathbb{R}} \frac{1}{\pi(1 + \xi^2)} \mathcal{T} e^{i \int_0^t (\xi H_1(s) + H_2(s)) ds} \mathbf{u}_0 d\xi,$$

which is the exact formula in [4, Theorem 1], and it can be seen as a special recovery from Schrödingerization.

3.2. Implementation on a quantum device. From (2.9), $|\mathbf{w}_h(t)\rangle$ can be computed by

$$(3.9) \quad |\mathbf{w}_h(T)\rangle = (\Phi \otimes I_n) \mathcal{U}(T) (\Phi^{-1} \otimes I_n) |\mathbf{w}_h(0)\rangle,$$

where $\mathcal{U}(T)$ is a unitary operator, given by

$$\mathcal{U}(T) = \mathcal{T} \exp(-i \int_0^T H^d(s) ds),$$

and Φ (or Φ^{-1}) is completed by (inverse) quantum Fourier transform (QFT or IQFT)[34]. The Hamiltonian simulation with respect to \mathcal{U} can be implemented as in [5, 7, 8, 9, 13, 12, 35, 33, 36].

3.2.1. Computation cost for the measurements. After the Hamiltonian simulation, one can recover the target variables for \mathbf{u} by performing a measurement in the computational basis:

$$M_k = |k\rangle\langle k| \otimes I, \quad k \in \mathcal{I}_\diamond,$$

where $\mathcal{I}_\diamond = \{j : p^\diamond \leq p_j \leq p^\diamond + R\}$ is referred to as the recovery index set. The state vector is then collapsed to

$$|\mathbf{u}_*\rangle \equiv |k_*\rangle \otimes \frac{1}{\mathcal{N}} \left(\sum_i w_{k_*i} |i\rangle \right), \quad \mathcal{N} = \left(\sum_i |w_{k_*i}|^2 \right)^{1/2},$$

for some k_* in the recovery index set \mathcal{I}_\diamond with the probability

$$\text{Pr}(T, p_{k_*}) = \frac{\sum_i |w_{k_*i}(T)|^2}{\sum_{k,i} |w_{ki}(T)|^2} \approx \frac{\|\mathbf{w}(T, p_{k_*})\|^2}{\sum_k \|\mathbf{w}(T, p_k)\|^2}.$$

Then the likelihood of acquiring $|\mathbf{u}_*\rangle$ that satisfies $k_* \in \mathcal{I}_\diamond$ is given by

$$\text{Pr}^* = \frac{\sum_{k \in \mathcal{I}_\diamond, i} |w_{ki}(T)|^2}{\sum_{k,i} |w_{ki}(T)|^2} \approx \frac{C_{e0}^2 \|\mathbf{u}(T)\|^2}{C_e^2 \|\mathbf{u}(0)\|^2},$$

where

$$(3.10) \quad C_{e0} = \left(\sum_{(p^\diamond \leq p_k \leq (p^\diamond + R))} e^{-2|p_k|} \right)^{1/2}, \quad C_e = \left(\sum_{k=0}^{N_p-1} e^{-2|p_k|} \right)^{1/2}.$$

If N_p is sufficiently large, we have

$$\Delta p C_{e0}^2 \approx \int_{p^\diamond}^{p^\diamond+R} e^{-2p} dp = \frac{1}{2} e^{-2p^\diamond} (1 - e^{-2R}), \quad \Delta p C_e^2 \approx \int_{-\infty}^{\infty} e^{-2p} dp = 1.$$

Since $R \geq 1$, it yields $\frac{C_{e0}^2}{C_e^2} \approx \frac{1}{2} e^{-2p^\diamond} (1 - e^{-2R}) > \frac{2}{5} e^{-2p^\diamond}$. By using the amplitude amplification, the repeated times for the measurements can be approximated as

$$(3.11) \quad g = \mathcal{O}\left(\frac{C_e \|\mathbf{u}(0)\|}{C_{e0} \|\mathbf{u}(T)\|}\right) = \mathcal{O}\left(e^{p^\diamond} \frac{\|\mathbf{u}(0)\|}{\|\mathbf{u}(T)\|}\right).$$

Remark 3.3. If all the eigenvalue of H_1 are negative, then one has $p^\diamond = 0$ and $C_e/C_{e0} = \mathcal{O}(1)$. Conversely, if H_1 possesses positive eigenvalues, the solution exhibits exponential growth with $\|\mathbf{u}(T)\| = \mathcal{O}(e^{p^\diamond} \|\mathbf{u}_0\|)$, which consequently implies $g = \mathcal{O}(1)$. For the backward heat equation discussed in [28], the parameter p^\diamond is selected to truncate high-frequency Fourier modes — a choice that does not inherently require p^\diamond to be large; detailed justifications are provided in [28].

The continuous or analog version is also similar, and it is possible in principle to implement $\mathbf{u} = e^{p^\diamond} \int_{p^\diamond}^{\infty} \mathbf{w}(p) dp$ directly without discretisation in the p domain, using the smooth projective operator $\int_{p^\diamond}^{\infty} f(p) |p\rangle \langle p| dp$, where $f(p)$ can model imperfections in the detection device. The probability of recovering the desired quantum state $\mathbf{u}(t)/\|\mathbf{u}(t)\|$ is then $(\int_{p^\diamond}^{\infty} f(p) dp \|\mathbf{u}(t)\|/\|\mathbf{u}(0)\|)^2$ [24].

3.3. Turning a non-autonomous system into an autonomous one. Recently, a new method was proposed in [15] which can turn any non-autonomous unitary dynamical system into an autonomous unitary system. First, via Schrödingerization, one obtains a time-dependent Hamiltonians

$$(3.12) \quad \frac{d}{dt} \mathbf{w}_h = -iH(t)\mathbf{w}_h, \quad H = H^\dagger.$$

By introducing a new “time” variable s , the problem becomes a new linear PDE defined in one higher dimension but with time-independent coefficients,

$$(3.13) \quad \frac{\partial \mathbf{v}}{\partial t} = -\frac{\partial \mathbf{v}}{\partial s} - iH(s)\mathbf{v} \quad \mathbf{v}(0, s) = \delta(s)\mathbf{w}_h(0), \quad s \in \mathbb{R},$$

where $\delta(s)$ is a dirac δ -function. One can easily recover \mathbf{w}_h by $\mathbf{w}_h = \int_{-\infty}^{\infty} \mathbf{v}(t, s) ds$.

3.3.1. The discrete Fourier transform. Since v decays to zero as s approaches infinity, the s -region can be truncated to $[-\pi S, \pi S]$, where $\pi S > 4\omega + T$, with 2ω representing the length of the support set of the approximated delta function. Choosing S sufficiently large ensures that the compact support of the approximated delta function remains entirely within the computational domain throughout the simulation, allowing the spectral method to be applied. The transformation and difference matrix are defined by

$$(\Phi_s)_{lj} = (e^{i\mu_l^s(j\Delta s)}), \quad D_s = \text{diag}\{\mu_0^s, \mu_1^s, \dots, \mu_{N_s-1}^s\}, \quad \mu_l^s = (l - \frac{N_s}{2})S, \quad l, j \in [N_s],$$

where $\Delta s = 2\pi S/N_s$. Applying the discrete Fourier spectral discretization, it yields a time-independent system as

$$(3.14) \quad \frac{d}{dt} \tilde{\mathbf{v}}_h = -i(D_s \otimes I + I_N \otimes H^d) \tilde{\mathbf{v}}_h, \quad \tilde{\mathbf{v}}_h(0) = [\Phi_s^{-1} \otimes I](\delta_h \otimes \tilde{\mathbf{w}}_h(0)),$$

where $\delta_{\mathbf{h}} = \sum_{j \in [N_s]} \delta_{\omega}(s_j) |j\rangle$ with $s_j = -\pi S + j\Delta s$ and δ_{ω} is an approximation to δ function defined, for example, by choosing

$$\delta_{\omega}(x) = \frac{1}{\omega} \left(1 - \frac{1}{2} \left| 1 + \cos\left(\pi \frac{x}{\omega}\right) \right| \right) \quad |x| \leq \omega, \quad \delta_{\omega}(x) = 0 \quad |x| \geq \omega.$$

Here $\omega = m\Delta s$, where m is the number of mesh points within the support of δ_{ω} .

3.3.2. The continuous Fourier transform. For a continuous-variable formulation, one can choose δ_{ω} to be a Gaussian function

$$\delta_{\omega}(x) = \frac{1}{\sqrt{2\pi\omega^2}} e^{-x^2/(2\omega^2)}.$$

The Fourier transform of δ_{ω} is given by

$$\hat{\delta}_{\omega}(\hat{x}) = \frac{1}{2\pi} \int_{\mathbb{R}} e^{i\hat{x}x} \delta_{\omega}(x) dx = \frac{1}{2\pi} e^{-\frac{(\omega\hat{x})^2}{2}}.$$

Since $\hat{\delta}_{\omega}$ decays exponentially in phase space, we only need to truncate the \hat{x} interval to a finite domain $[-\hat{X}, \hat{X}]$, where the truncation size \hat{X} satisfies $\hat{X} = \mathcal{O}(\ln \epsilon^{-1})$. Applying the continuous Fourier spectral discretization, one gets the time-*independent* Hamiltonian

$$(3.15) \quad \frac{d}{dt} \tilde{\mathbf{v}}_h = i(D_{\hat{x}} \otimes I + I \otimes H^c) \tilde{\mathbf{v}}_h, \quad \tilde{\mathbf{v}}_h(0) = \hat{\delta}_h \otimes \tilde{\mathbf{w}}_h(0),$$

where $D_{\hat{x}} = \text{diag}\{\hat{x}_0, \hat{x}_1, \dots, \hat{x}_{N_{\hat{x}}}\}$ and $\hat{\delta}_h = \frac{1}{2\pi} \sum_{j=0}^{N_{\hat{x}}} e^{-\frac{(\hat{x}_j \omega)^2}{2}} |j\rangle$, $\hat{x}_j = -\hat{X} + 2\hat{X}j/N_{\hat{x}}$ and $\omega = 2\hat{X}/N_{\hat{x}}$.

From (3.14) and (3.15), it is easy to find the evolution matrices are time independent.

4. Error estimates for the discretizations of the Schrödingerized system. In this section, we establish rigorous error bounds for the discrete formulations of the Schrödingerized system, corresponding to the numerical schemes (2.9) and (2.12), respectively.

4.1. Error estimates for (2.9) . Define the complex $(N_p + 1)$ dimensional space with respect to p

$$X_{N_p}^p = \text{span}\{e^{ik(p/L)} : -N_p/2 \leq k \leq N_p/2\}.$$

The approximation of \mathbf{w} in the finite space $X_{N_p}^p$ from the numerical solution in (2.9) is

$$(4.1) \quad \mathbf{w}_h^d(t, p) = \sum_{|k| \leq N_p/2} \tilde{\mathbf{w}}_{j_k} e^{ik(\frac{t}{L} + \pi)}, \quad \tilde{\mathbf{w}}_{j_k} = (\langle j_k | \otimes I) \tilde{\mathbf{w}}_h(t),$$

where $j_k = -k + N_p/2$. Correspondingly, the approximation of \mathbf{u} is defined by

$$(4.2) \quad \mathbf{u}_h^d(t, p) = e^p \mathbf{w}_h^d(t, p) \quad p \in (p^{\diamond}, p^{\diamond} + R).$$

From (4.2), we observe that to estimate the error between \mathbf{u}_h^d and \mathbf{u} , it suffices to bound the error between \mathbf{w}_h^d and \mathbf{w} . It is apparent that the discretization serves as an approximation for the following system with periodic boundaries:

$$(4.3) \quad \begin{cases} \frac{d}{dt}\mathcal{W} = -H_1\partial_p\mathcal{W} + iH_2\mathcal{W}, & 0 \leq t \leq T, \\ \mathcal{W}(t, -\pi L) = \mathcal{W}(t, \pi L), \\ \mathcal{W}(0, p) = \mathcal{G}(p)\mathbf{u}_0, \end{cases}$$

where \mathcal{G} is periodic with a period of $2\pi L$, such that

$$\mathcal{G}(p) = e^{-[p-(j+1)\pi L]} \quad j\pi L \leq p < (j+2)\pi L, \quad j \in \mathbb{Z}.$$

Since $\mathcal{W} \in H^1(\Omega_p)$ is periodic, the standard estimate of spectral methods shows

$$(4.4) \quad \|\mathbf{w}_h^d(T, p) - \mathcal{W}(T, p)\|_{L^2(\Omega_p)} \lesssim \Delta p \|\mathcal{W}(T, p)\|_{H^1(\Omega_p)} \lesssim \Delta p \|\mathbf{u}(T)\|.$$

In order to estimate the error between \mathbf{w}_h^d and \mathbf{w} , it is sufficient to analyze the error between \mathbf{w} and \mathcal{W} .

LEMMA 4.1. *Assume $H(t), H_u(t) \in \mathbb{C}^{n,n}$ are Hermitian matrices, and $\mathbf{v} \in \mathbb{C}^n$ satisfies*

$$\frac{d}{dt}\mathbf{v} = i(H + H_u)\mathbf{v}, \quad \mathbf{v}(0) = \mathbf{v}_0.$$

Then, there exists a unitary matrix U_H such that

$$(4.5) \quad \mathbf{v}(t) = \mathcal{T} e^{i \int_0^t H(s) ds} U_H(t) \mathbf{v}_0.$$

Proof. Differentiating both sides of (4.5) with respect to t , it is easy to observe that $U_H(t)$ satisfies

$$(4.6) \quad \frac{d}{dt}U_H(t) = i\mathcal{T} e^{-i \int_0^t H(s) ds} H_u \mathcal{T} e^{i \int_0^t H(s) ds} U_H = iV(t)U_H, \quad U_H(0) = I.$$

The proof is finished by noting that $V(t)$ is Hermitian. \square

LEMMA 4.2. *Let $\mathcal{E}(t, p) = \mathcal{W}(t, p) - \mathbf{w}(t, p)$, it follows that*

$$(4.7) \quad \int_0^T \mathcal{E}^\dagger(t, -\pi L) H_1 \mathcal{E}(t, -\pi L) dt \lesssim e^{-2\pi L + 2\lambda_{\max}^+(H_1)T} \|\mathbf{u}_0\|^2,$$

$$(4.8) \quad \int_0^T \mathcal{E}^\dagger(t, \pi L) H_1 \mathcal{E}(t, \pi L) dt \lesssim e^{-2\pi L + 2\lambda_{\max}^-(H_1)T} \|\mathbf{u}_0\|^2.$$

Proof. Since H_1 is Hermitian, there exists a unitary $U(t)$ such that $H_1(t) = U(t)\Sigma(t)(U(t))^\dagger$, where $\Sigma(t) = \text{diag}\{\lambda_1(t), \dots, \lambda_n(t)\}$. Introducing the change of variable $\mathbf{w}_u = U^\dagger \mathbf{w}$, one gets the equation of $\hat{\mathbf{w}}_u = \mathcal{F}(\mathbf{w}_u)$ as

$$\frac{d}{dt}\hat{\mathbf{w}}_u = i\xi\Sigma\hat{\mathbf{w}}_u + iH_u\hat{\mathbf{w}}_u,$$

where $H_u = UH_2U^\dagger - \partial_t U U^\dagger / i$ is Hermitian. Here we have used the fact that $\partial_t U U^\dagger$ is skew-symmetric. From Lemma 4.1, by choosing $p = -\pi L$, one has

$$\mathbf{w}(t, -\pi L) = \int_{\mathbb{R}} U(t) \Lambda^w(t, \xi) U_H(t, \xi) U^\dagger(0) \mathbf{u}_0 d\xi,$$

where $\Lambda^w(t, \xi)$ is a diagonal matrix with diagonal entries

$$\Lambda_{jj}^w = \frac{1}{\pi(1 + \xi^2)} e^{i\xi(\int_0^t \lambda_j(s) ds + \pi L)},$$

and $U_H(t, \xi)$ is a unitary matrix, satisfying

$$\frac{d}{dt} U_H = i\mathcal{T} e^{-i \int_0^t \xi \Sigma(s) ds} H_u \mathcal{T} e^{i \int_0^t \xi \Sigma(s) ds} U_H, \quad U_H(0) = I.$$

Similarly, one gets

$$\mathcal{W}(t, -\pi L) = \int_{\mathbb{R}} U(t) \Lambda^{\mathcal{W}}(t, \xi) U_H(t, \xi) U^\dagger(0) \mathbf{u}_0 d\xi,$$

with $\Lambda^{\mathcal{W}}(t, \xi)$ the diagonal matrix,

$$\Lambda_{jj}^{\mathcal{W}}(t, \xi) = \hat{\mathcal{G}}(\xi) e^{i\xi(\int_0^t \lambda_j(s) ds + \pi L)}.$$

Letting $\mathcal{E}(t, p) = \mathcal{W}(t, p) - \mathbf{w}(t, p)$ and noting U_H is unitary, careful calculation gives

$$\begin{aligned} (4.9) \quad & \int_0^T \mathcal{E}^\dagger(t, -\pi L) H_1 \mathcal{E}(t, -\pi L) dt \\ &= \int_0^T \mathbf{u}_0^\dagger U(0) \left(\int_{\mathbb{R}} U_H^\dagger (\Lambda^{\mathcal{W}} - \Lambda^w) \Sigma(t) (\Lambda^{\mathcal{W}} - \Lambda^w) U_H d\xi \right) U^\dagger(0) \mathbf{u}_0 dt \\ &\leq \|\Lambda\| \|\mathbf{u}_0\|^2, \end{aligned}$$

where the diagonal matrix Λ is defined by

$$\Lambda = \int_0^T \int_{\mathbb{R}} (\Lambda^{\mathcal{W}} - \Lambda^w) \Sigma(t) (\Lambda^{\mathcal{W}} - \Lambda^w) d\xi dt.$$

It follows from the inverse Fourier transform that the diagonal entries of Λ are

$$\Lambda_{jj} = \int_0^T \left(e^{-|\int_0^t \lambda_j(s) ds + \pi L|} - \mathcal{G}\left(-\int_0^t \lambda_j(s) ds - \pi L\right) \right)^2 \lambda_j(t) dt.$$

Changing the variable of integration by letting $q = \int_0^t \lambda_j(s) ds + \pi L$, and recalling the definition of \mathcal{G} , it yields

$$(4.10) \quad \Lambda_{jj} = \int_{\pi L}^{\pi L + \int_0^T \lambda_j(s) ds} (e^{-|q|} - \mathcal{G}(-q))^2 dq \lesssim e^{-2\pi L + 2\lambda_{\max}^+(H_1)T} + e^{-2\pi L}.$$

The proof for (4.7) is completed by inserting (4.10) into (4.9). The proof for (4.8) is similar, which is omitted here. \square

LEMMA 4.3. Assume $\mathbf{w}(t, p)$ and $\mathcal{W}(t, p)$ are defined in (2.3) and (4.3), respectively, it follows that

$$\|\mathbf{w}(T, p) - \mathcal{W}(T, p)\|_{L^2(\Omega_p)} \lesssim (e^{-\pi L + \lambda_{\max}^+(H_1)T} + e^{-\pi L + \lambda_{\max}^-(H_1)T}) \|\mathbf{u}_0\|.$$

Proof. By introducing $\mathcal{E}(t, p) = \mathcal{W}(t, p) - \mathbf{w}(t, p)$, one has

$$(4.11) \quad \frac{d}{dt} \mathcal{E} = -H_1 \partial_p \mathcal{E} + iH_2 \mathcal{E}, \quad \mathcal{E}(0, p) = \begin{cases} \mathbf{0}, & \text{in } \Omega_p \\ \mathcal{G} - e^{-|p|}, & \text{in } \mathbb{R} \setminus \Omega_p \end{cases}.$$

Testing (4.11) against \mathcal{E}^\dagger and integrating by parts, it yields

$$\int_0^T \frac{d}{dt} \|\mathcal{E}\|_{L^2(\Omega_p)}^2 = - \int_0^T \mathcal{E}^\dagger(t, \pi L) H_1 \mathcal{E}(t, \pi L) + \int_0^T \mathcal{E}^\dagger(t, -\pi L) H_1 \mathcal{E}(t, -\pi L).$$

Since H_1 may have negative eigenvalues, one has

$$\|\mathcal{E}(T, p)\|_{L^2(\Omega_p)}^2 \leq \left| \int_0^T \mathcal{E}^\dagger(t, \pi L) H_1 \mathcal{E}(t, \pi L) \right| + \left| \int_0^T \mathcal{E}^\dagger(t, -\pi L) H_1 \mathcal{E}(t, -\pi L) \right|.$$

The proof is finished by using Lemma 4.2. \square

From Theorem 3.1, we may regard \mathbf{u} as a function with respect to the variable p . With these preparations, we are now ready to present the main result of this subsection.

THEOREM 4.4. *Suppose πL satisfies (2.5) with ϵ the desired accuracy. Assume \mathbf{u}_h^d is defined in (4.2). There holds*

$$\|\mathbf{u}_h^d(T) - \mathbf{u}(T)\|_{L^2(\tilde{\Omega}_p)} \lesssim \Delta p e^{p^\diamond} \|\mathbf{u}(T)\| + \epsilon \|\mathbf{u}_0\|,$$

where $\tilde{\Omega}_p = (p^\diamond, p^\diamond + R)$, $R \geq 1$ is the length of the recovery region with $e^R = \mathcal{O}(1)$.

Proof. According to the recovery rule in Theorem 3.1, it follows that

$$\|\mathbf{u} - \mathbf{u}_h^d\|_{L^2(\tilde{\Omega}_p)} = \|e^p \mathbf{w} - e^p \mathbf{w}_h^d\|_{L^2(\tilde{\Omega}_p)}.$$

From the triangle equality, Lemma 4.3 and (4.4), it yields

$$\begin{aligned} \|\mathbf{u} - \mathbf{u}_h^d\|_{L^2(\tilde{\Omega}_p)} &\leq \|e^p \mathcal{W} - e^p \mathbf{w}_h^d\|_{L^2(\tilde{\Omega}_p)} + \|e^p \mathbf{w} - e^p \mathcal{W}\|_{L^2(\tilde{\Omega}_p)} \\ &\lesssim \Delta p e^{p^\diamond + R} \|\mathbf{u}(T)\| + e^{-\pi L + p^\diamond + R} (e^{\lambda_{\max}^+(H_1)T} + e^{\lambda_{\max}^-(H_1)T}) \|\mathbf{u}_0\|. \end{aligned}$$

The proof is finished by considering $e^R = \mathcal{O}(1)$ and (2.5). \square

Remark 4.5. It is noted from Theorem 4.4, the limitation of the convergence order mainly comes from the non-smoothness of the initial values. In order to improve the whole convergence rates, we change the initial value of $\mathbf{w}(0)$ as $\mathbf{w}(0) = \psi(p) \mathbf{u}_0$, where $\psi(p) \in H^r(\mathbb{R})$ satisfies $\psi(p) = e^{-p}$ for $p \geq 0$. Thus $\mathcal{W}, \mathbf{w} \in \mathbf{H}^r(\Omega_p)$ and the error estimate implies

$$(4.12) \quad \|\mathbf{u}_h^d(T) - \mathbf{u}(T)\|_{L^2(\tilde{\Omega}_p)} \lesssim \Delta p^r e^{p^\diamond} \|\mathbf{u}(T)\| + \epsilon \|\mathbf{u}_0\|.$$

The explicit construction of $\psi(p)$ is given in [28, section 4.3]. For $r = 2$, a smoother initial function is given by

$$(4.13) \quad \psi(p) = \begin{cases} (-3 + 3e^{-1})p^3 + (-5 + 4e^{-1})p^2 - p + 1 & p \in (-1, 0), \\ e^{-|p|} & \text{otherwise.} \end{cases}$$

Assuming that L is sufficiently large and the grid size $\Delta p = \mathcal{O}(\sqrt{\epsilon})$ is sufficiently small, we can eliminate the constants hidden in the notation of \lesssim in (4.12), resulting in the following formula:

$$(4.14) \quad \|\mathbf{u}(T) - \mathbf{u}_*\| \leq \frac{\epsilon}{4} \|\mathbf{u}(T)\|,$$

where $\mathbf{u}_* = e^{p k_*} (\langle k_* | \otimes I) \mathbf{w}_h$, $k_* \in \mathcal{I}_\diamond$. The extra qubits needed due to the extra dimension are $\mathcal{O}(\log(\frac{L}{\sqrt{\epsilon}}))$. Since r can be arbitrarily large, the number of qubits required for the smooth extension in p -dimensional space achieves a nearly exponential reduction compared to the original Schrödingerization.

4.2. Error estimates for (2.12). The approximation for \mathbf{w} is computed by

$$(4.15) \quad \mathbf{w}_h^c = \Delta \xi \sum_{j=1}^{N-1} \check{\mathbf{w}}_j e^{-i\xi_j p} + \frac{\Delta \xi}{2} (\check{\mathbf{w}}_N e^{-i\xi_N p} + \check{\mathbf{w}}_0 e^{-i\xi_0 p}).$$

Here $\check{\mathbf{w}}_j = (\langle j | \otimes I_n) \check{\mathbf{w}}_h$. Without considering the error of quantum simulation, one gets $\check{\mathbf{w}}_j = \hat{\mathbf{w}}(t, \xi_j)$, $\xi_j = -X + 2jX/N$. It is obvious to see that \mathbf{w}_h^c is the numerical integration of $\int_{-X}^X e^{-i\xi p} \hat{\mathbf{w}} d\xi \approx \int_{\mathbb{R}} e^{-i\xi p} \hat{\mathbf{w}} d\xi$. Then, we define the approximation to \mathbf{u} by

$$(4.16) \quad \mathbf{u}_h^c(t, p) = e^p \mathbf{w}_h^c(t, p) \quad p \in (p^\diamond, p^\diamond + R).$$

LEMMA 4.6. *The error estimate for (2.3) computed by (2.12) is given by*

$$(4.17) \quad \|\mathbf{w}_h^c(T, p) - \mathbf{w}(T, p)\| \lesssim (X^{-1} + X \Delta \xi^2 \|H_p^2\|) \|\mathbf{u}_0\| \quad p > p^\diamond,$$

where $H_p = \int_0^T H_1(s) ds - pI$.

Proof. The error estimate for (2.3) by (2.12) consists of two parts. The first part is from the truncation of ξ domain. From the definition of $\mathcal{U}_{t,0}(\xi)$ in (3.2), it yields

$$\|\mathcal{U}_{t,0}(\xi) e^{-i\xi p}\| \leq 1.$$

The truncation error is then bounded by

$$(4.18) \quad \left\| \int_{(-\infty, -X] \cup [X, \infty)} \frac{\mathcal{U}_{t,0}(\xi)}{\pi(1+\xi^2)} e^{-i\xi p} \mathbf{u}_0 d\xi \right\| \leq \int_X^\infty \frac{2\|\mathbf{u}_0\|}{\pi(1+\xi^2)} d\xi \lesssim X^{-1} \|\mathbf{u}_0\|.$$

The second part is from the numerical integration. Write $F(t, \xi, p) = \frac{\mathcal{U}_{t,0}(\xi)}{\pi(1+\xi^2)} e^{-i\xi p}$ and $H_p = \int_0^t H_1(s) ds - pI$, one then has

$$\partial_\xi^2 F(t, \xi, p) = \left(-\frac{H_p^2}{\pi(1+\xi^2)} - \frac{4i\xi H_p + 2}{\pi(1+\xi^2)^2} + \frac{8\xi^2}{\pi(1+\xi^2)^3} \right) \mathcal{T} e^{i \int_0^t \xi(H_1 - \frac{p}{t}I) + H_2(s) ds}.$$

According to the error estimate of numerical quad, there exists $\xi^* \in [-X, X]$ such that

$$(4.19) \quad \left\| \mathbf{w}_h^c - \int_{-X}^X \frac{e^{-i\xi p} \mathcal{U}_{t,0}(\xi) \mathbf{u}_0}{\pi(1+\xi^2)} d\xi \right\| = \frac{\Delta \xi^2 X}{6} \|\partial_\xi^2 F(t, \xi^*, p)\| \|\mathbf{u}_0\| \lesssim \Delta \xi^2 X \|H_p^2\| \|\mathbf{u}_0\|.$$

The proof is completed by the triangle inequality from (4.18) and (4.19). \square

Integrating the inequality of (4.17), the error between \mathbf{u}_h^c and \mathbf{u} is shown as follows.

THEOREM 4.7. *Assume X satisfies (2.11), \mathbf{u}_h^c is defined in (4.16). It follows that*

$$(4.20) \quad \|\mathbf{u}_h^c - \mathbf{u}\|_{L^2(\tilde{\Omega}_p)} \lesssim \left(\epsilon + \epsilon^{-1} \Delta \xi^2 ((p^\diamond)^2 + \left\| \int_0^T H_1(s) ds \right\|^2) \right) e^{p^\diamond} \|\mathbf{u}_0\|,$$

where $\tilde{\Omega}_p = (p^\diamond, p^\diamond + R)$, and $R \geq 1$ is the length of the recovery domain with $e^R = \mathcal{O}(1)$.

Remark 4.8. It is noted that the first part ϵ dominates in (4.20) when $\Delta\xi$ is small enough such that $\Delta\xi \lesssim \epsilon/\sqrt{(p^\diamond)^2 + \|\int_0^T H_1(s)ds\|^2}$. By using the Fourier transform of smoother initial data, we no longer need to truncate the interval at $X = \mathcal{O}(1/\epsilon)$, and can instead use the much smaller cutoff $X = \mathcal{O}(\log(1/\epsilon)^{1/\beta})$, $\beta \in (0, 1)$. This leads to an exponential reduction in the Hamiltonian simulation time caused by the extra dimension with respect to ϵ when compared to the original formula (2.12) [1].

4.3. Complexity analysis. In order to get the total query complexity, we need to obtain the cost of simulating the time-evolution operator $\mathcal{U}(T)$. Since a time-dependent system can be made autonomous (see section 3.3), we focus on the time-independent cost of $\mathcal{U}(T)$ for the discrete Fourier transform of Schrödingerization. The complexity of the continuous Fourier transform is similar to [1] and is omitted here. We introduce the complexity of Hamiltonian simulation in [21] by QSVT.

LEMMA 4.9 (Complexity of block-Hamiltonian simulation). *Let $\epsilon \in (0, \frac{1}{2})$, $t \in \mathbb{R}$, and $\alpha \in \mathbb{R}^+$. Let U be an $(\alpha, a, 0)$ -block-encoding of the unknown Hamiltonian H . To implement an ϵ -precise Hamiltonian simulation unitary V that is a $(1, a + 2, \epsilon)$ -block-encoding of e^{itH} , the unitary U must be queried*

$$(4.21) \quad \Theta\left(\frac{\alpha|t| + \log(1/\epsilon)}{\log(e + \log(1/\epsilon)/(\alpha|t|))}\right)$$

times.

Finally, we obtain the complexity of our algorithm based on Lemma 4.9, error estimates and repeated times discussed in section 3.2.1.

THEOREM 4.10. *Assume that $\psi \in H^r(\mathbb{R})$ is smooth enough, πL is large enough and $\Delta p = \mathcal{O}(\sqrt[3]{\epsilon})$ is small enough to satisfy (4.14) with ϵ the desired precision. There exists a quantum algorithm that prepares an ϵ -approximation of the state $|\mathbf{u}\rangle$ with $\Omega(1)$ success probability and a flag indicating success, using*

$$\tilde{\mathcal{O}}\left(e^{p^\diamond} \frac{\|\mathbf{u}(0)\|}{\|\mathbf{u}(T)\|} \left(\frac{T\alpha_H}{\sqrt[3]{\epsilon}} + \log \frac{e^{p^\diamond} \|\mathbf{u}(0)\|}{\epsilon^{1/r+1} \|\mathbf{u}(T)\|}\right)\right)$$

queries, where $\alpha_H \geq \|H_i\|, i = 1, 2$.

Proof. Based on the Hamiltonian simulation, the state \mathbf{w}^a/η_0 can be prepared with $\eta_0 = \|\mathbf{w}_h(0)\|$, yielding the approximation state vector $|\mathbf{u}^a(T)\rangle$ for the solution $|\mathbf{u}(T)\rangle$. The error between $|\mathbf{u}\rangle$ and $|\mathbf{u}^a(T)\rangle$ is obtained by

$$\| |\mathbf{u}(T)\rangle - |\mathbf{u}^a(T)\rangle \| \leq \| |\mathbf{u}(T)\rangle - |\mathbf{u}_*\rangle \| + \| |\mathbf{u}_*\rangle - |\mathbf{u}^a(T)\rangle \|,$$

where $\mathbf{u}_* = e^{p_{k_*}}(\langle k_*| \otimes I)\mathbf{w}_h$, $k_* \in \mathcal{I}_\diamond$. From (4.14), one has

$$\| |\mathbf{u}(T)\rangle - |\mathbf{u}_*\rangle \| \leq 2\|\mathbf{u}(T) - \mathbf{u}_*\|/\|\mathbf{u}(T)\| \leq \epsilon/2.$$

Neglecting the error in the implementation of $\mathcal{U}(T)$, there holds

$$(4.22) \quad \| |\mathbf{u}_*\rangle - |\mathbf{u}^a(T)\rangle \| \leq 2\|\mathbf{u}_* - \mathbf{u}^a\|/\|\mathbf{u}_*\| \leq 2e^{p_{k_*}}\|\mathbf{w}_h - \mathbf{w}^a\|/\|\mathbf{u}_*\|.$$

To ensure the overall error remains within ϵ , we require $\| |\mathbf{u}_*\rangle - |\mathbf{u}^a\rangle \| \leq \epsilon/2$, yielding

$$(4.23) \quad \| |\mathbf{w}_h\rangle - |\mathbf{w}^a\rangle \| \leq 2\frac{\|\mathbf{w}_h - \mathbf{w}^a\|}{\|\mathbf{w}_h\|} \leq \frac{\epsilon e^{-p_{k_*}} \|\mathbf{u}_*\|}{2\eta_0} \approx \frac{\epsilon e^{-p_{k_*}} \|\mathbf{u}(T)\|}{\Delta p \|\mathbf{u}(0)\|} := \delta.$$

According to Lemma 4.9, the assumption of mesh size and (4.23), the time cost to implement $\mathcal{U}(T)$ is

$$\tilde{\mathcal{O}}\left(T\|H^d\| + \log \frac{1}{\delta}\right) = \tilde{\mathcal{O}}\left(\frac{T\alpha_H}{\sqrt[r]{\epsilon}} + \log \frac{e^{p^\diamond}\|\mathbf{u}(0)\|}{\epsilon^{1/r+1}\|\mathbf{u}(T)\|}\right).$$

The proof is finished by multiplying the repeated times shown in (3.11). \square

Remark 4.11. Since r can be arbitrarily large and we use spectral methods to discretize in the p -direction, the dependence on $1/\epsilon$ can be reduced to a logarithmic level, i.e., the query complexity approaches $\tilde{\mathcal{O}}(e^{p^\diamond} \frac{\|\mathbf{u}(0)\|}{\|\mathbf{u}(T)\|} T\alpha_H \log \frac{1}{\epsilon})$. Following the analysis in [1], we derive the complexity of the continuous Fourier transform as $\tilde{\mathcal{O}}(e^{p^\diamond} \frac{\|\mathbf{u}(0)\|}{\|\mathbf{u}(T)\|} T\alpha_H (\log \frac{1}{\epsilon})^{1/\beta})$, where β is a real parameter satisfying $0 < \beta < 1$.

5. The inhomogenous problem. In this section, we consider the problem with inhomogeneous source term, i.e. $\mathbf{b}(t) \neq \mathbf{0}$ in (1.1). Define $\tilde{A} \in \mathbb{C}^{2n \times 2n}$ by $\tilde{A} = \begin{bmatrix} A & B \\ O & O \end{bmatrix}$ and $H_1^A = (A + A^\dagger)/2$, $H_2^A = (A - A^\dagger)/(2i)$. There holds $\tilde{A} = \tilde{H}_1 + i\tilde{H}_2$, with \tilde{H}_1 and \tilde{H}_2 both Hermitian, where \tilde{H}_1 and \tilde{H}_2 are defined by

$$(5.1) \quad \tilde{H}_1 = \begin{bmatrix} H_1^A & \frac{B}{2} \\ \frac{B^\top}{2} & O \end{bmatrix}, \quad \tilde{H}_2 = \begin{bmatrix} H_2^A & \frac{B}{2i} \\ -\frac{B^\top}{2i} & O \end{bmatrix}.$$

Apply the Schrödingerization to (2.1), it leads to

$$(5.2) \quad \frac{d}{dt} \mathbf{w}_f = -\tilde{H}_1 \partial_p \mathbf{w}_f + i\tilde{H}_2 \mathbf{w}_f, \quad \mathbf{w}_f(0) = \psi(p) \begin{bmatrix} \mathbf{u}_0 \\ \mathbf{r}_0 \end{bmatrix}.$$

5.1. The eigenvalues of \tilde{H}_1 impacted by the inhomogeneous term. Assume H_1^A and \tilde{H}_1 have n and $2n$ real eigenvalues, respectively, such that

$$(5.3) \quad \lambda_1(H_1^A) \leq \lambda_2(H_1^A) \leq \dots \leq \lambda_n(H_1^A), \quad \lambda_1(\tilde{H}_1) \leq \lambda_2(\tilde{H}_1) \leq \dots \leq \lambda_{2n}(\tilde{H}_1),$$

for all $t \in [0, T]$.

LEMMA 5.1. Assume $\mathbf{b} \neq \mathbf{0}$, then there exist both positive and negative eigenvalues of \tilde{H}_1 .

Proof. We first consider the case that H_1^A is invertible. After elementary row and column operations, one has

$$(5.4) \quad \begin{bmatrix} I & O \\ -\frac{B^\top (H_1^A)^{-1}}{2} & I \end{bmatrix} \tilde{H}_1 \begin{bmatrix} I & \frac{(H_1^A)^{-\top} B}{2} \\ O & I \end{bmatrix} = \begin{bmatrix} H_1^A & O \\ O & -\frac{B^\top (H_1^A)^{-1} B}{4} \end{bmatrix} = \tilde{H}_1^{RC}.$$

According to (5.4), it follows that $\lambda(\tilde{H}_1^{RC}) = \{\lambda(H_1^A), -\lambda(B^\top (H_1^A)^{-1} B)/4\}$ have both positive and negative values. Since the matrix \tilde{H}_1 has the same number of positive eigenvalues and the same number of negative eigenvalues as the matrix \tilde{H}_1^{RC} , the statement is proved.

Next we consider the case that H_1^A is not invertible. The following proof is from eigenvalue inequalities for Hermitian matrices [22, Corollary 4.3.15], that is for any Hermitian matrices $H_A, H_B \in \mathbb{C}^{n,n}$, then

$$(5.5) \quad \lambda_i(H_A) + \lambda_1(H_B) \leq \lambda_i(H_A + H_B) \leq \lambda_i(H_A) + \lambda_n(H_B), \quad i = 1, \dots, n.$$

Let $H_N^* = H_1^A - \delta_0 I$, with $\delta_0 = 2 \max\{|\lambda(H_1^A)|\}$. Then H_N^* is negative. By letting $\tilde{H}_N^* = \begin{bmatrix} H_N^* & B/2 \\ B^\top/2 & O \end{bmatrix}$, it follows immediately from what we have proved that there exists i_0 such that $\lambda_{i_0}(\tilde{H}_N^*) > 0$. From (5.5), it is easy to see that $\lambda_{i_0}(\tilde{H}_1) \geq \lambda_{i_0}(\tilde{H}_N^*) > 0$. Similarly, there exists j_0 such that $\lambda_{j_0}(\tilde{H}_1) \leq \lambda_{j_0}(\tilde{H}_P^*) < 0$, where $\tilde{H}_P^* = \begin{bmatrix} H_P^* & B/2 \\ B^\top/2 & O \end{bmatrix}$ with $H_P^* = H_1^A + \delta_0 I$. \square

LEMMA 5.2. *The eigenvalues of \tilde{H}_1 satisfy*

$$(5.6) \quad |\lambda_{i_k}(\tilde{H}_1) - \lambda_k(H_1^A)| \leq \frac{|b|}{2} \quad \text{and} \quad |\lambda_{j_k}(\tilde{H}_1)| \leq \frac{|b|}{2}, \quad 1 \leq i_k \leq 2n, \quad 1 \leq k \leq n,$$

where $|b| = \max_t \|\mathbf{b}\|_{l^\infty}$, and the indices satisfy $j_k \in \{1, 2, \dots, 2n\} \setminus (\{i_k\}_{k=1}^n)$.

Proof. The result will be proved from (5.5). We complete the proof by observing that

$$(5.7) \quad \tilde{H}_1 = \tilde{H}_{11} + \tilde{H}_{12} = \begin{bmatrix} H_1^A & O \\ O & O \end{bmatrix} + \begin{bmatrix} O & \frac{B}{2} \\ \frac{B^\top}{2} & O \end{bmatrix},$$

with $|b|/2$ and $-|b|/2$ the maximum and minimum eigenvalues of \tilde{H}_{12} . \square

5.2. Turning an inhomogeneous system into a homogeneous one. From Lemma 5.1, it can be seen that the presence of the source term will destroy the negative definiteness of matrix H_1^A . Then we alleviate this defect by rescaling the auxiliary vector \mathbf{r} with \mathbf{r}/γ , where

$$(5.8) \quad \gamma = 1/(C_T |b|), \quad |b| = \max_t \|\mathbf{b}\|_{l^\infty}.$$

Here, C_T is a parameter that satisfies $C_T = \mathcal{O}(1)$ and is larger than the evolution time. If the evolution time T is known, we can set $C_T = T$. The new linear system is

$$(5.9) \quad \frac{d}{dt} \mathbf{u}_f^\gamma = A^\gamma \mathbf{u}_f, \quad A_f = \begin{bmatrix} A & \gamma B \\ O & O \end{bmatrix}, \quad \mathbf{u}_f(0) = \begin{bmatrix} \mathbf{u}_0 \\ \mathbf{r}_0/\gamma \end{bmatrix}.$$

Define

$$H_1^\gamma = \begin{bmatrix} H_1^A & \frac{\gamma B}{2} \\ \frac{\gamma B^\top}{2} & O \end{bmatrix}, \quad H_2^\gamma = \begin{bmatrix} H_2^A & \frac{\gamma B}{2i} \\ -\frac{\gamma B^\top}{2i} & O \end{bmatrix}.$$

Using the Schrödingerization method, one gets

$$(5.10) \quad \frac{d}{dt} \mathbf{w}_f^\gamma = -H_1^\gamma \partial_p \mathbf{w}_f^\gamma + i H_2^\gamma \mathbf{w}_f^\gamma, \quad \mathbf{w}_f^\gamma(0) = e^{-|p|} \begin{bmatrix} \mathbf{u}_0 \\ \mathbf{r}_0/\gamma \end{bmatrix}.$$

From Theorem 3.1, one could choose $p > p^{\gamma, \diamond}$ to recover \mathbf{u}_f^γ from \mathbf{w}_f^γ , where

$$(5.11) \quad p^{\gamma, \diamond} = p^\diamond + \mathcal{O}(\gamma |b| T) = \lambda_{\max}^+(H_1^A) T + \mathcal{O}(1).$$

Then, we arrive at the recovery theorem for the inhomogeneous case.

THEOREM 5.3. Assume the eigenvalues of H_1^A satisfy (5.3) and γ satisfies (5.8), we have

$$\mathbf{u} = e^p(\langle 0| \otimes I)\mathbf{w}_f^\gamma, \quad p > p^{\gamma, \diamond},$$

where $p^{\gamma, \diamond}$ is given in (5.11), or use the integration to get

$$\mathbf{u} = e^p(\langle 0| \otimes I) \int_p^\infty \mathbf{w}_f^\gamma(q) dq, \quad p > p^{\gamma, \diamond}.$$

5.2.1. Discretization of the Schrödingerized system. Applying the discrete Fourier transform to (5.10) gives

$$(5.12) \quad \frac{d}{dt} \tilde{\mathbf{w}}_{f,h}^\gamma = -i(D_p \otimes H_1^\gamma - I \otimes H_2^\gamma) \tilde{\mathbf{w}}_{f,h}^\gamma, \quad \tilde{\mathbf{w}}_{f,h}^\gamma = (\Phi^{-1} \otimes I)(\psi_h \otimes \begin{bmatrix} \mathbf{u}_0 \\ C_T |b| \mathbf{r}_0 \end{bmatrix}),$$

where $\psi_h = \sum_{k \in [N_p]} e^{-|p_k|} |k\rangle$ and $p_k = -\pi L + 2k\pi L/N_p$. Here πL is large enough to satisfy

$$(5.13) \quad e^{-\pi L + 2\lambda_{\max}^+(H_1^A)T + R + 1} \leq \epsilon, \quad e^{-\pi L + \lambda_{\max}^-(H_1^A)T + \lambda_{\max}^+(H_1^A) + R + 1} \leq \epsilon,$$

with $R \geq 1$ and $e^R = \mathcal{O}(1)$. Then, the Hamiltonian simulation can be performed.

According to Theorem 4.4, we get the error estimate of system in (5.12).

COROLLARY 5.4. Assume πL is large enough and satisfies (5.13). The approximation \mathbf{u}_h^d is defined by

$$\mathbf{u}_h^d(T, p) = e^p \sum_{|k| \leq N_p/2} (\langle j_k | \otimes I) \tilde{\mathbf{w}}_{f,h}^\gamma e^{ik(p/L + \pi)} \quad p \in \tilde{\Omega}_p,$$

where $j_k = -k + \frac{N_p}{2}$ and $\tilde{\Omega}_p = (p^{\gamma, \diamond}, p^{\gamma, \diamond} + R)$. Then, it yields

$$\|\mathbf{u}_h^d - \mathbf{u}\|_{L^2(\tilde{\Omega}_p)} \lesssim \Delta p e^{p^\diamond} (\|\mathbf{u}(T)\| + C_T \|\mathbf{b}\|) + \epsilon (\|\mathbf{u}_0\| + C_T \|\mathbf{b}\|),$$

where $\|\mathbf{b}\| = |b| \|\mathbf{r}_0\|$.

Since $\mathbf{u}_f^\gamma = \begin{bmatrix} \mathbf{u} \\ \mathbf{r}/\gamma \end{bmatrix}$, one can perform a projection to get $|\mathbf{u}(T)\rangle$ with the probability $\frac{\|\mathbf{u}(T)\|^2}{\|\mathbf{u}_f^\gamma(T)\|^2}$. According to the analysis of the computation cost for the measurement in section 3.2.1, the overall probability for getting $|\mathbf{u}(T)\rangle$ is approximated by

$$P_u = \frac{C_{e0,\gamma}^2 \|\mathbf{u}(T)\|^2}{C_{e,\gamma}^2 \|\mathbf{u}_f^\gamma(0)\|^2} = \frac{C_{e0,\gamma}^2}{C_{e,\gamma}^2} \frac{\|\mathbf{u}(T)\|^2}{\|\mathbf{u}(0)\|^2 + C_T^2 \|\mathbf{b}\|^2},$$

where $\|\mathbf{b}\| = |b| \|\mathbf{r}_0\|$, and $\frac{C_{e0,\gamma}}{C_{e,\gamma}} \approx \sqrt{\frac{(1-e^{-2})e^{-2p^{\gamma, \diamond}}}{2}} \geq 0.65e^{-p^{\gamma, \diamond}}$. By using the amplitude amplification, the repeated times for the measurements can be approximated as

$$(5.14) \quad g \approx e^{p^\diamond + 1} \frac{\sqrt{\|\mathbf{u}(0)\|^2 + C_T^2 \|\mathbf{b}\|^2}}{\|\mathbf{u}(T)\|}.$$

As shown in Theorem 4.10, for smooth initial data and with γ selected as in (5.8), the Hamiltonian simulation of (5.12) achieves a query complexity of nearly $\tilde{\mathcal{O}}(e^{p^\diamond} \frac{\sqrt{\|\mathbf{u}(0)\|^2 + C_T^2 \|\mathbf{b}\|^2}}{\|\mathbf{u}(T)\|} (T\alpha_H \log \frac{1}{\epsilon}))$, where $\alpha_H \geq \|H_i^A\|$, $i = 1, 2$.

By using the Fourier transform in p of \mathbf{w}_f^γ , it yields

$$(5.15) \quad \frac{d}{dt} \hat{\mathbf{w}}_f^\gamma = i(\xi H_1^\gamma + H_2^\gamma) \hat{\mathbf{w}}_f^\gamma = iH^\gamma \hat{\mathbf{w}}_f^\gamma,$$

where $\hat{\mathbf{w}}_f^\gamma = \mathcal{F}(\mathbf{w}_f^\gamma)$. Here $H^\gamma(\xi)$ is Hermitian for any $\xi \in \mathbb{R}$. From Lemma 5.2, one has $\lambda(H_1^\gamma) = \lambda(H_1^A) + \mathcal{O}(1)$.

By applying the continuous Fourier transform to the Schrödingerization framework (see (5.15)), we truncate the ξ -domain to $[-X, X]$ for numerical implementation, yielding

$$(5.16) \quad \frac{d}{dt} \check{\mathbf{w}}_{f,h}^\gamma = i(D_\xi \otimes H_1^\gamma + I \otimes H_2^\gamma) \check{\mathbf{w}}_{f,h}^\gamma, \quad \check{\mathbf{w}}_{f,h}^\gamma = \boldsymbol{\xi}_h \otimes \begin{bmatrix} \mathbf{u}_0 \\ C_T |b| \mathbf{r}_0 \end{bmatrix},$$

where D_ξ and $\boldsymbol{\xi}_h$ are defined in the same way as in (2.12). Following Theorem 4.6, one gets the error estimate for (5.16).

COROLLARY 5.5. *Assume \mathbf{w}_h^c is obtained by (4.15) with the solution to (5.16), and $\mathbf{u}_h^c = e^p \mathbf{w}_h^c$. Additionally, X is large enough to satisfy (2.11). Then there holds*

$$\|\mathbf{u}_h^c - \mathbf{u}\|_{L^2(\tilde{\Omega}_p)} \lesssim \left(\epsilon + \frac{1}{\epsilon} \Delta \xi^2 ((p^\diamond)^2 + \left\| \int_0^T (H_1^A(s) ds \right\|^2) \right) e^{p^\diamond} (\|\mathbf{u}_0\| + C_T \|\mathbf{b}\|),$$

where $\|\mathbf{b}\| = |b| \|\mathbf{r}_0\|$ and $\tilde{\Omega}_p = (p^{\gamma, \diamond}, p^{\gamma, \diamond} + R)$.

Remark 5.6. Our algorithm by using (5.12) focuses on direct quantum state preparation of

$$\mathbf{u}_* = e^{p_{k*}} (\langle k_* | \otimes \langle 0 | \otimes I) \mathbf{w}_{f,h}^\gamma,$$

with $\mathbf{w}_{f,h}^\gamma = (\Phi^{-1} \otimes I) \hat{\mathbf{w}}_{f,h}^\gamma$, enabling the computation of a wide range of physical quantities. To estimate the quantum observable $\langle \mathbf{u}_* | S | \mathbf{u}_* \rangle$ associated with the quadratic form $\mathbf{u}^\dagger S \mathbf{u}$, we proceed as follows. Given access to a block-encoding U_S of the operator S , both the real and imaginary components of $\mathbf{u}_*^\dagger S \mathbf{u}_*$ can be efficiently computed. Specifically, these quantities are obtained via the Hadamard test technique [42], where the real component corresponds to the standard protocol and the imaginary part is extracted by introducing a $\pi/2$ -phase shift in the ancilla qubit rotation. To get the quantum observable after computing (5.16), the process can be found in [4].

6. Numerical tests. In this section, we use several examples to verify our theory and show the correctness of the mathematical formulation. All of the numerical tests are performed in the classical computers by using Crank-Nicolson method for temporal discretization.

6.1. Recovery from Schrödingerization. In this test, we use the following scattering model-like problem in $[0, 2]$ to test the recovery from Schrödingerization,

$$(6.1) \quad \partial_t u = \Delta u + k^2 u, \quad u(0) = \sin(\pi x),$$

with zero boundary conditions. The exact solution is $u = e^{(k^2 - \pi^2)t} \sin(\pi x)$, and we use $k = 4$. The spatial discretization is given by the finite difference method,

$$\frac{d}{dt} \mathbf{u} = A \mathbf{u}, \quad A = \begin{bmatrix} \alpha & \beta & & & \\ \beta & \alpha & \beta & & \\ & \ddots & \ddots & \ddots & \\ & & \beta & \alpha & \beta \\ & & & \beta & \alpha \end{bmatrix}, \quad \alpha = -\frac{2}{h^2} + k^2, \quad \beta = \frac{1}{h^2}.$$

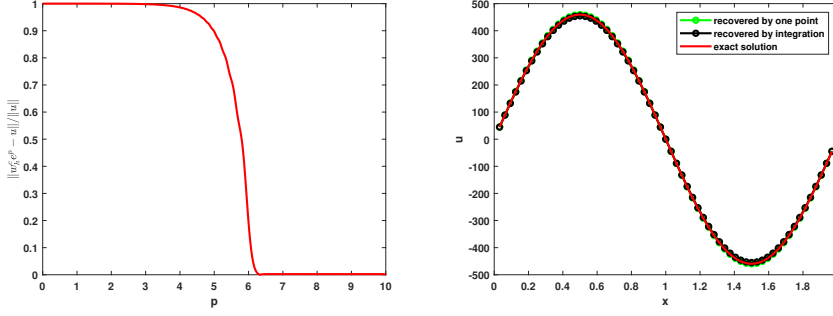


FIG. 1. Left: error of $\|\mathbf{u} - \mathbf{w}_h^c(p)e^p\|/\|\mathbf{u}\|$ with respect to p with \mathbf{w}_h^c computed by (4.15). Right: the recovery from Schrödingerization by choosing $p > p^\diamond = \lambda_n(H_1)T \approx 6$.

The computation stops at $T = 1$. One can check that the eigenvalues of A are $\lambda_j(A) = \frac{1}{h^2}(-2 + 2\cos(\frac{j\pi}{n+1})) + k^2$, $j = 1, \dots, n$. It can be seen that the eigenvalue of A may be positive when k is large. In this test, we observe $\lambda_{\max}^+(A) \approx 6$ when $h = 1/2^5$ numerically. From the plot on the left in Fig. 1, it can be seen that the error between \mathbf{u} and $\mathbf{w}_h^c e^p$ drops precipitously at $p^\diamond = \lambda_{\max}^+(H_1)T \approx 6$. Here \mathbf{w}_h^c is computed using (2.12), with ξ truncated to the interval $(-80, 80)$, $\Delta\xi = \frac{5}{24}$ and $\Delta t = \frac{1}{2^5}$. According to Theorem 3.1, we should choose $p > p^\diamond \approx 6$ to recover \mathbf{u} . The results are shown on the right of Fig. 1, where the numerical solutions recovered by selecting a single point or numerical integration are close to the exact solutions.

6.2. Recovery from Schrödingerization for ill-posed problems. In this test, we use the backward heat equation in $[0, 2]$, with the Dirichlet boundary condition $u(t, 0) = u(t, 2) = 0$, to test the recovery from Schrödingerization,

$$\partial_t u = -\Delta u, \quad u(0, x) = \exp(-25\pi^2) \sin\left(\frac{\pi}{2}x\right).$$

The exact solution is given by $u(t, x) = \exp(\frac{\pi^2}{4}t - 25\pi^2) \sin(\frac{\pi}{2}x)$. It is well known that the backward heat equation is unstable, which is hard to simulate. Applying the Schrödingerization yields

$$(6.2) \quad \frac{d}{dt}w = \Delta \partial_p w, \quad w(0, x, p) = e^{-|p|}u(0, x).$$

By using the Fourier transform technique to (6.2) with respect to the variables p and x , which correspond to Fourier modes ξ and η , respectively, one gets the Fourier transform $\hat{w}(t, \eta, \xi)$ of the exact solution $w(t, x, p)$ of problem (6.2) satisfying

$$\frac{d}{dt}\hat{w} = -i\xi\eta^2\hat{w}, \quad \hat{w}(0) = \hat{w}_0 = \frac{\hat{u}_0(\eta)}{\pi(1 + \xi^2)},$$

where $\hat{u}_0(\eta) = \mathcal{F}(u_0) = \frac{1}{2\pi} \int_{\mathbb{R}} e^{ix\eta} u(0, x) dx$. The solution of w is then found to be

$$w(T, x, p) = \frac{1}{2i} \int_{\mathbb{R}} e^{-|p - \eta^2 T|} e^{-ix\eta - 25\pi^2} \left(\delta\left(\eta + \frac{\pi}{2}\right) - \delta\left(\eta - \frac{\pi}{2}\right) \right) d\eta.$$

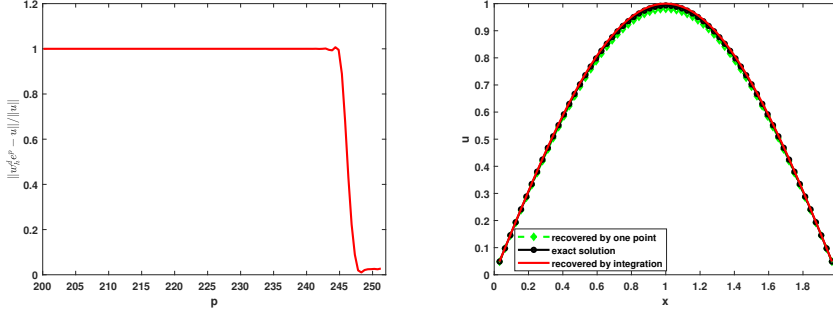


FIG. 2. Left: error of $\|\mathbf{u} - \mathbf{w}_h^d(p)e^p\|$ with respect to p with \mathbf{w}_h^d defined in (4.1). Right: the recovery from Schrödingerization by choosing $p > p^\diamond = \frac{\pi^2}{4}T \approx 247$.

Since \hat{u}_0 has a compact support, namely $\hat{u}_0 = 0$ for $|\eta| \geq \frac{\pi}{2}$. To recover $u(T, x)$, we need to choose $p > \frac{\pi^2}{4}T$, resulting in

$$u(T, x) = e^p \int_{-\frac{\pi}{2}}^{\frac{\pi}{2}} e^{-(p-\eta^2 T)} \hat{u}_0 e^{-ix\eta} d\eta = \int_{\mathbb{R}} e^{\eta^2 T} \hat{u}_0 e^{-ix\eta} d\eta, \quad p > \frac{\pi^2}{4}T.$$

The computation stops at $T = 100$, which represents a relatively long duration for an unstable system. In this work, we apply the Schrödingerization method to partial differential equations, followed by spatial discretization with $p \in \Omega_p = (-257, 257)$, $\Delta x = \frac{1}{25}$, $\Delta p = \frac{257}{29}$ and $\Delta t = \frac{25}{210}$. This method fully exploits the exponential decay property in Fourier space. The magnitude of p^\diamond is $\mathcal{O}(T)$. For more details on selecting p^\diamond to recover the solution of the ill-posed system and the corresponding error analysis, we refer to [28]. The results are shown on the right side of Fig. 2, where the numerical solutions recovered either by selecting a single point or through numerical integration are close to the exact solution. The error $\|\mathbf{u} - \mathbf{w}_h^d(p)e^p\|$ with respect to p is illustrated on the left side of Fig. 2, demonstrating that by appropriately choosing the interval $(p^\diamond, p^\diamond + R)$ with $e^R = \mathcal{O}(1)$ and $p^\diamond = \pi^2 T/4$, the target solution can be effectively recovered.

Classical methods with traditional regularization techniques, such as filtering or other approaches [37, 41], require careful parameter selection: too small leads to instability, too large results in excessive smoothing and loss of details. In contrast, Schrödingerization, as guaranteed by Theorem 3.1, provides accurate (modulus truncation of high-frequency modes of the initial data) approximations with precise error estimates from the perspective of continuous functions. While similar to Fourier regularization [20], our method is simpler to implement. A detailed comparison is provided in [28].

6.3. Convergence rates of the discretization for Schrödingerized systems. In these tests, we use the numerical simulation to test the convergence rates of the discretization of Schrödingerization and compare different discretization schemes for the Schrödingerized equations.

First, we consider a 1-D case for Maxwell's equations. For the three-dimensional case, a similar approach can be adopted straightforwardly [27]. The electric field is assumed to have a transverse component E_y , i.e. $\mathbf{E} = (0, E_y(x, t), 0)$. The magnetic field is aligned with the z direction and its magnitude is denoted by B_z , i.e. $\mathbf{B} =$

TABLE 1
The convergence rates of $\frac{\|\mathbf{u}_h^d - \mathbf{u}\|_{L^2(\tilde{\Omega}_p)}}{\|\mathbf{u}\|_{L^2(\tilde{\Omega}_p)}}$ and $\frac{\|\mathbf{u}_h^c - \mathbf{u}\|_{L^2(\tilde{\Omega}_p)}}{\|\mathbf{u}\|_{L^2(\tilde{\Omega}_p)}}$, with $\gamma = 0.1$ and $\tilde{\Omega}_p = (\frac{1}{2}, \frac{3}{2})$.

$(\Delta p, \Delta t)$	$(\frac{\pi}{2^7}, \frac{1}{2^8})$	order	$(\frac{\pi}{2^8}, \frac{1}{2^9})$	order	$(\frac{\pi}{2^9}, \frac{1}{2^{10}})$	order
$\frac{\ \mathbf{u}_h^d(p) - \mathbf{u}(p)\ _{L^2(\tilde{\Omega}_p)}}{\ \mathbf{u}\ _{L^2(\tilde{\Omega}_p)}}$	4.50e-05	-	1.33e-05	1.75	3.28e-06	2.02
$(X, \Delta t)$	$(80, \frac{1}{2^8})$	order	$(160, \frac{1}{2^9})$	order	$(320, \frac{1}{2^{10}})$	order
$\frac{\ \mathbf{u}_h^c(p) - \mathbf{u}(p)\ _{L^2(\tilde{\Omega}_p)}}{\ \mathbf{u}\ _{L^2(\tilde{\Omega}_p)}}$	1.74e-03	-	4.67e-04	1.90	1.78e-04	1.39

$(0, 0, B_z(x, t))$. The reduced Maxwell system with periodic boundary conditions is written as

$$(6.3) \quad \partial_t E_y + \partial_x B_z = -J_y, \quad \partial_t B_z + \partial_x E_y = 0, \quad \text{in } [0, 1].$$

The simulation stops at $T = 1$.

6.3.1. An in-homogeneous system with source terms. The source term is defined as

$$J_y(t, x) = -2\pi t \cos(2\pi x).$$

The initial conditions are prescribed as follows

$$E_y(0, x) = \cos(2\pi x)/(2\pi) - 1/(2\pi), \quad B_z(0, x) = 0.$$

The exact solution to the system is given by

$$E_y = \cos(2\pi x)/(2\pi) - 1/(2\pi), \quad B_z = t \sin(2\pi x).$$

Yee's scheme [40] for spatial discretization gives

$$\frac{d}{dt} \begin{bmatrix} \mathbf{u} \\ \mathbf{r} \end{bmatrix} = \begin{bmatrix} A & B \\ O & O \end{bmatrix} \begin{bmatrix} \mathbf{u} \\ \mathbf{r} \end{bmatrix},$$

where $\mathbf{u} = \sum_{i=0}^{n-2} E_{i+1} |i\rangle + \sum_{i=0}^{n-1} B_{i+\frac{1}{2}} |n-1+i\rangle$ and $\mathbf{r} = \sum_{i=0}^{n-2} |i\rangle$. The matrix $A \in \mathbb{R}^{2n-1, 2n-1}$ and $B \in \mathbb{R}^{2n-1, n-1}$ are defined by

$$A = \begin{bmatrix} O & -D_x \\ D_x^\top & O \end{bmatrix}, \quad B = \begin{bmatrix} -J_y \\ \mathbf{0} \end{bmatrix}, \quad D_x = \frac{1}{h} \begin{bmatrix} 1 & -1 & 0 & \cdots & 0 \\ & 1 & -1 & \cdots & 0 \\ & & \ddots & \ddots & \\ & & & 1 & -1 \end{bmatrix} \in \mathbb{R}^{n-1, n},$$

where $\mathbf{J}_y = \text{diag}\{\mathbf{J}_h\}$ with $\mathbf{J}_h = \sum_{i=1}^{n-1} J_y(x_i, t) |i\rangle$. Then \tilde{H}_1 is obtained by $\tilde{H}_1 = \begin{bmatrix} O & B/2 \\ B/2 & O \end{bmatrix}$. Obviously, one gets $\lambda(\tilde{H}_1) = \mathcal{O}(|b|/2) = \mathcal{O}(\max_{x,t}\{J_y\}/2)$.

In this test, we choose $\gamma = 0.1$ and the modified smooth initial values (4.13) to test the convergence rates of the discretization for Schrödingerization. For (5.12), we fix the p -domain within $\Omega_p = (-\pi, \pi)$. For (5.16), we fix the step size of ξ

with $\Delta\xi = \frac{5}{2^3}$ and $\tilde{\Omega}_p = (\frac{1}{2}, \frac{3}{2})$. Tab. 1 shows that the optimal convergence order $\|\mathbf{u}_h^d - \mathbf{u}\|_{L^2(\tilde{\Omega}_p)} \sim \Delta p^2$ and $\|\mathbf{u}_h^c - \mathbf{u}\|_{L^2(\tilde{\Omega}_p)} \sim X^{-1}$ are obtained, respectively. Fig. 3 shows $\|\mathbf{w}_h^c e^p - \mathbf{u}\|$ and $\|\mathbf{w}_h^d e^p - \mathbf{u}\|$ with respect to p . It implies that it is better to pick the point $p > p^\diamond$ near p^\diamond , to avoid the error being magnified exponentially for large p when using a single point to recover \mathbf{u} by $\mathbf{u}_h^d = e^p \mathbf{w}_h^d$ (or $\mathbf{u}_h^c = e^p \mathbf{w}_h^c$). According to the proof in Theorem 4.6, the residual of $\mathbf{w}_h^c - \mathbf{w}$ contains $\int e^{i\xi p} d\xi$, leading to the oscillation of $\|\mathbf{w}_h^c e^p - \mathbf{u}\|$ in terms of p . Therefore, it would be better to apply integration to recover \mathbf{u} when using continuous Fourier transformation for Schrödingerization.

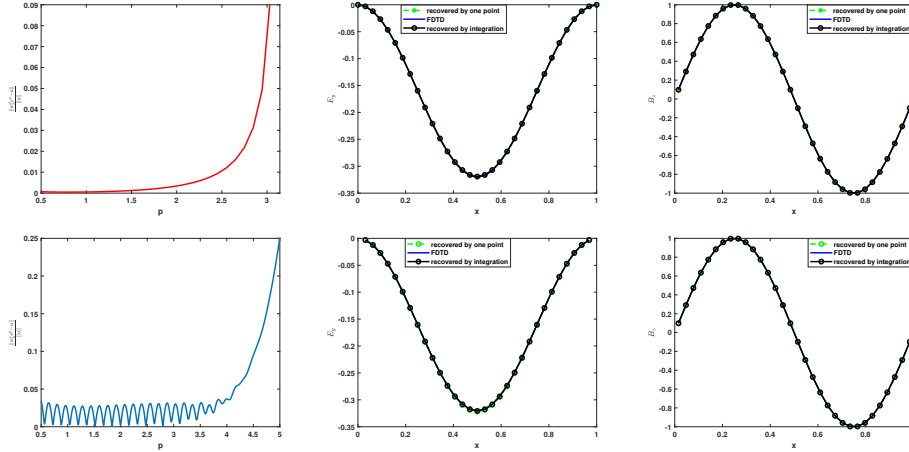


FIG. 3. The first row: the error of discrete Fourier transform defined by $\|\mathbf{w}_h^d e^p - \mathbf{u}\|/\|\mathbf{u}\|$ for Schrödingerization, with $\Delta p = \frac{\pi}{2^5}$ and $\Delta t = \frac{1}{2^5}$. The second row: the error of continuous Fourier transform defined by $\|\mathbf{w}_h^c e^p - \mathbf{u}\|/\|\mathbf{u}\|$ for Schrödingerization, with $X = 160$ and $\Delta t = \frac{1}{2^5}$.

6.3.2. An in-homogeneous system with big source terms. In this test, we fix the initial conditions of (6.3) and modify the source term as

$$J_y = -2000\pi t \cos(2\pi x).$$

It is straightforward to observe that $\lambda(\tilde{H}_1) = \mathcal{O}(10^3)$, making it challenging to recover without employing the stretch transformation. By choosing $\gamma = 10^{-4}$, the recovery from Schrödingerization agrees well with the exact solution (see Fig. 4). Comparing Tab. 1 and Tab. 2, we find that the stretch coefficient does not affect the relative error and the convergence order.

By comparing the results of section 6.3.1 and section 6.3.2, we make the following summary.

- **Compare two discretizations of Schrödingerization :** (2.9) and (2.12). When $\lambda_{\max}^-(H_1)$ is not particularly large, we refer to (2.9) to discretize the Schrödingerized equations. Compared with (2.12), the discrete Fourier transform for Schrödingerization (2.9) has a smaller error and higher-order convergence rates from Tab. 1. However, large $\lambda_{\max}^-(H_1)$ requires a particularly large p domain for the discrete Fourier transform and very small $\Delta\xi$ for the continuous Fourier transform (2.12).
- **Compare two recovery methods:** (3.3) and (3.4). According to Fig. 3

TABLE 2
The convergence rates of $\frac{\|\mathbf{u}_h^d - \mathbf{u}\|_{L^2(\tilde{\Omega}_p)}}{\|\mathbf{u}\|_{L^2(\tilde{\Omega}_p)}}$ and $\frac{\|\mathbf{u}_h^c - \mathbf{u}\|_{L^2(\tilde{\Omega}_p)}}{\|\mathbf{u}\|_{L^2(\tilde{\Omega}_p)}}$, with $\gamma = \frac{1}{10^4}$ and $\tilde{\Omega}_p = (\frac{1}{2}, \frac{3}{2})$.

$(\Delta p, \Delta t)$	$(\frac{\pi}{2^8}, \frac{1}{2^7})$	order	$(\frac{\pi}{2^9}, \frac{1}{2^8})$	order	$(\frac{\pi}{2^9}, \frac{1}{2^{10}})$	order
$\frac{\ \mathbf{u}_h^d(p) - \mathbf{u}(p)\ _{L^2(\tilde{\Omega}_p)}}{\ \mathbf{u}\ _{L^2(\tilde{\Omega}_p)}}$	4.09e-05	-	1.21e-05	1.75	2.99e-06	2.02
$(X, \Delta t)$	$(80, \frac{1}{2^8})$	order	$(160, \frac{1}{2^9})$	order	$(320, \frac{1}{2^{10}})$	order
$\frac{\ \mathbf{u}_h^c(p) - \mathbf{u}(p)\ _{L^2(\tilde{\Omega}_p)}}{\ \mathbf{u}\ _{L^2(\tilde{\Omega}_p)}}$	1.58e-03	-	4.14e-04	1.93	1.32e-04	1.64

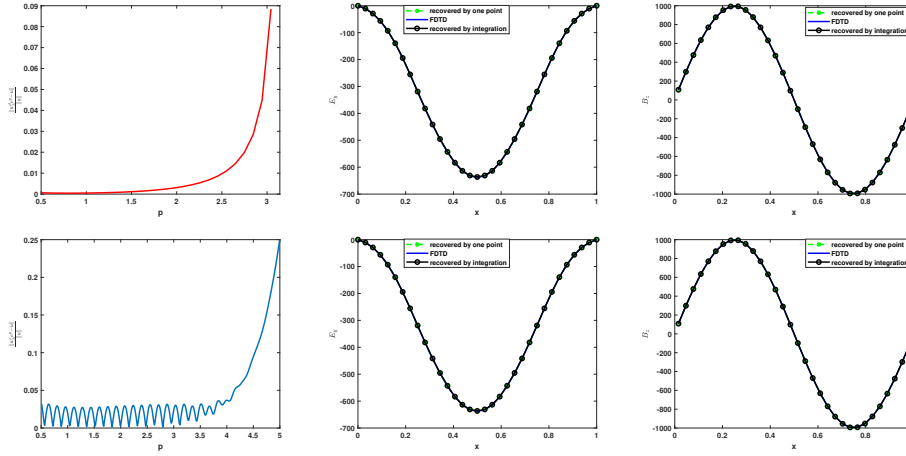


FIG. 4. The first row: the error of discrete Fourier transform defined by $\|\mathbf{w}_h^d e^p - \mathbf{u}\|$ for Schrödingerization, with $\Delta p = \frac{\pi}{2^5}$ and $\Delta t = \frac{1}{2^5}$. The second row: the error of continuous Fourier transform defined by $\|\mathbf{w}_h^c e^p - \mathbf{u}\|$ for Schrödingerization, with $X = 160$ and $\Delta t = \frac{1}{2^5}$.

and Fig. 4, the recovery of the primitive variables via a single point (i.e. (3.3)) is suitable for the discrete Fourier transform (2.9), and the recovery of the solution through integration (i.e. (3.4)) is suitable for the continuous Fourier transform (2.12), due to the oscillations of the error with p .

7. Conclusions. In this paper, we present some analysis and numerical investigations of the Schrödingerization of a general linear system with a source term. Conditions under which to recover the original variables are studied theoretically and numerically, for systems that can contain unstable modes. We give the implementation details of the discretization of the Schrödingerization and prove the corresponding error estimates and convergence orders. In addition, we homogenize the source term by using the stretch transformation and show that the stretch coefficient does not affect the error estimate of the quantum simulation.

As can be seen from the analysis, it is difficult to recover the target variables when the evolution matrix has large positive eigenvalues, as in chaotic systems. Our method provides a simple and general way to construct stable (including both classical and quantum) computational methods for unstable, ill-posed problems. This will be the subject of our further investigation [28].

Acknowledgement. SJ and NL are supported by NSFC grant No. 12341104, the Shanghai Jiao Tong University 2030 Initiative and the Fundamental Research Funds for the Central Universities. SJ was also partially supported by the NSFC grants Nos. 12350710181 and 12426637, the Shanghai Municipal Science and Technology Major Project (2021SHZDZX0102). NL also acknowledges funding from the Science and Technology Program of Shanghai, China (21JC1402900). CM was partially supported by China Postdoctoral Science Foundation (No. 2023M732248) and Postdoctoral Innovative Talents Support Program (No. BX20230219).

REFERENCES

- [1] D. AN, A. M. CHILDS, AND L. LIN, *Quantum algorithm for linear non-unitary dynamics with near-optimal dependence on all parameters*, arXiv:2312.03916, (2023).
- [2] D. AN, D. FANG, AND L. LIN, *Time-dependent unbounded hamiltonian simulation with vector norm scaling*, Quantum, 5 (2021), p. 459.
- [3] D. AN, D. FANG, AND L. LIN, *Time-dependent hamiltonian simulation of highly oscillatory dynamics and superconvergence for schrödinger equation*, Quantum, 6 (2022), p. 690.
- [4] D. AN, J. LIU, AND L. LIN, *Linear combination of hamiltonian simulation for non-unitary dynamics with optimal state preparation cost*, Phys. Rev. Lett., 131 (2023), p. 150603.
- [5] D. W. BERRY, G. AHOKAS, R. CLEVE, AND B. C. SANDERS, *Efficient quantum algorithms for simulating sparse hamiltonians*, Commun. Math. Phys., 270 (2007), pp. 359–371.
- [6] D. W. BERRY AND A. M. CHILDS, *Black-box hamiltonian simulation and unitary implementation*, Quantum Inf. Comput., 12 (2012), pp. 39–62.
- [7] D. W. BERRY, A. M. CHILDS, R. CLEVE, R. KOTHARI, AND R. D. SOMMA, *Exponential improvement in precision for simulating sparse hamiltonians*, Proceedings of the 46th Annual ACM Symposium on Theory of Computing, (2014), pp. 283–292.
- [8] D. W. BERRY, A. M. CHILDS, R. CLEVE, R. KOTHARI, AND R. D. SOMMA, *Simulating hamiltonian dynamics with a truncated taylor series*, Phys. Rev. Lett., (2015), p. 090502.
- [9] D. W. BERRY, A. M. CHILDS, AND R. KOTHARI, *Hamiltonian simulation with nearly optimal dependence on all parameters*, IEEE 56th Annual Symposium on Foundations of Computer Science, (2015).
- [10] D. W. BERRY, A. M. CHILDS, Y. SU, X. WANG, AND N. WIEBE, *Time-dependent hamiltonian simulation with l_1 -norm scaling*, Quantum, 4 (2020), p. 254.
- [11] D. W. BERRY, R. CLEVE, AND S. GHARIBIAN, *Gate-efficient discrete simulations of continuous-time quantum query algorithms*, Quantum Inf. Comput., 14 (2014), pp. 1–30.
- [12] D. W. BERRY AND L. NOVO, *Corrected quantum walk for optimal hamiltonian simulation*, Quantum Inf. Comput., 16 (2016), p. 1295.
- [13] G. BRASSARD, P. HOYER, M. MOSCA, AND A. TAPP, *Quantum amplitude amplification and estimation*, Contemp. Math., 305 (2002), pp. 53–74.
- [14] E. CAMPBELL, *Random compiler for fast hamiltonian simulation*, Phys. Rev. Lett., 123 (2019).
- [15] Y. CAO, S. JIN, AND N. LIU, *Quantum simulation for time-dependent hamiltonians – with applications to non-autonomous ordinary and partial differential equations*, arXiv:2312.02817v1, (2023).
- [16] A. M. CHILDS, D. MASLOV, Y. NAM, N. J. ROSS, AND Y. SU, *Toward the first quantum simulation with quantum speedup*, Proc. Nat. Acad. Sci. India Sect. A, 115 (2018), pp. 9456–9461.
- [17] D. DIVINCENZO, *Quantum computation*, Science, 270 (1995), pp. 255–261.
- [18] A. EKERT, R. JOZSA, AND P. MARCER, *Quantum algorithms: Entanglement-enhanced information processing*, Philos. Trans. Royal Soc. A, 356 (1998), pp. 1769–1782.
- [19] L. C. EVANS, *Partial differential equations*, American Mathematical Society, (2016).
- [20] C. L. FU, X. T. XIONG, AND Z. QIAN, *Fourier regularization for a backward heat equation*, J. Math. Anal. Appl., 331 (2007), pp. 472–480.
- [21] A. GILYÉN, Y. SU, G. H. LOW, AND N. WIEBE, *Quantum singular value transformation and beyond: exponential improvements for quantum matrix arithmetics*, in Proceedings of the 51st Annual ACM SIGACT Symposium on Theory of Computing, 2019, pp. 193–204.
- [22] R. A. HORN AND C. R. JOHNSON, *Matrix analysis*, Cambridge University Press, (2012).
- [23] S. JIN, X. LI, N. LIU, AND Y. YU, *Quantum simulation for partial differential equations with physical boundary or interface conditions*, J. Comput. Phys., (2024), p. 112707.
- [24] S. JIN AND N. LIU, *Analog quantum simulation of partial differential equations*, Quantum Sci. Technol., 9 (2024), p. 035047.

- [25] S. JIN AND N. LIU, *Quantum simulation of discrete linear dynamical systems and simple iterative methods in linear algebra*, Proc. Roy. Soc. A, 480 (2024), p. 20230370.
- [26] S. JIN, N. LIU, X. LI, AND Y. YU, *Quantum simulation for quantum dynamics with artificial boundary conditions*, SIAM J. Sci. Comput., 46 (2024), pp. B403–B421.
- [27] S. JIN, N. LIU, AND C. MA, *Quantum simulation of maxwell’s equations via schrödingerisation*, ESAIM Math. Model. Numer. Anal., 58 (2024), p. 1853–1879.
- [28] S. JIN, N. LIU, AND C. MA, *Schrödingerisation based computationally stable algorithms for ill-posed problems in partial differential equations*, arXiv:2403.19123, (2024).
- [29] S. JIN, N. LIU, AND Y. YU, *Quantum simulation of partial differential equations via schrödingerisation: technical details*, arXiv:2212.14703, (2022).
- [30] S. JIN, N. LIU, AND Y. YU, *Quantum simulation of partial differential equations: Applications and detailed analysis*, Phys. Rev. A, 108 (2023), p. 032603.
- [31] S. JIN, N. LIU, AND Y. YU, *Quantum simulation of partial differential equations via Schrödingerization*, Phys. Rev. Lett., 133 (2024), p. 230602.
- [32] C. S. LAM, *Decomposition of time-ordered products and path-ordered exponentials*, J. Math. Phys., 39 (1998), pp. 5543–5558.
- [33] G. H. LOW AND I. L. CHUANG, *Optimal hamiltonian simulation by quantum signal processing*, Phys. Rev. Lett., 118 (2017), p. 010501.
- [34] M. A. NIELSEN AND I. L. CHUANG, *Quantum computation and quantum information*, Cambridge University Press, (2000).
- [35] L. NOVO AND D. W. BERRY, *Improved hamiltonian simulation via a truncated taylor series and corrections*, Quantum Inf. Comput., 17 (2017), p. 0623.
- [36] D. POULIN, A. QARRY, R. D. SOMMA, AND F. VERSTRAETE, *Quantum simulation of time-dependent hamiltonians and the convenient illusion of hilbert space*, Phys. Rev. Lett., 106 (2011), p. 170501.
- [37] T. I. SEIDMAN, *Optimal filtering for the backward heat equation*, SIAM J. Numer. Anal., 33 (1996), pp. 162–170.
- [38] P. W. SHOR, *Algorithms for quantum computation: Discrete logarithms and factoring*, Proceedings 35th Annual Symposium on Foundations of Computer Science, (1994), pp. 124–134.
- [39] A. STEANE, *Quantum computing*, Rep. Progr. Phys., 61 (1998), pp. 117–173.
- [40] A. TAFLOVE, S. C. HAGNESS, AND M. PIKET-MAY, *Computational electromagnetics: The finite-difference time-domain method*, The Electrical Engineering Handbook, 3 (2005), pp. 629–670.
- [41] F. TERNAT, O. ORELLANA, AND P. DARIPA, *Two stable methods with numerical experiments for solving the backward heat equation*, Appl. Numer. Math., 61 (2011), pp. 266–284.
- [42] Y. TONG, D. AN, N. WIEBE, AND L. LIN, *Fast inversion, preconditioned quantum linear system solvers, fast Green’s-function computation, and fast evaluation of matrix functions*, Phys. Rev. A, 66 (2021), pp. 2181–2188.
- [43] B. ŞAHINOĞLU AND R. D. SOMMA, *Hamiltonian simulation in the low-energy subspace*, npj Quantum Information, 7 (2021), p. 119.